Dartmouth College

Dartmouth Digital Commons

6-13-2014

Magnetic Inhibition of Convection and the Fundamental Properties of Low-Mass Stars. Ii. Fully Convective Main-Sequence Stars

Gregory A. Feiden
Uppsala University

Brian Chaboyer
Dartmouth College

Follow this and additional works at: https://digitalcommons.dartmouth.edu/facoa

Part of the Astrophysics and Astronomy Commons

MAGNETIC INHIBITION OF CONVECTION AND THE FUNDAMENTAL PROPERTIES OF LOW-MASS STARS. II. FULLY CONVECTIVE MAIN-SEQUENCE STARS

Gregory A. Feiden[1] and Brian Chaboyer[2]
[1] Department of Physics and Astronomy, Uppsala University, Box 516, SE-751 20 Uppsala, Sweden; gregory.a.feiden@gmail.com
[2] Department of Physics and Astronomy, Dartmouth College, 6127 Wilder Laboratory, Hanover, NH 03755, USA; brian.chaboyer@dartmouth.edu

ABSTRACT

We examine the hypothesis that magnetic fields are inflating the radii of fully convective main-sequence stars in detached eclipsing binaries (DEBs). The magnetic Dartmouth stellar evolution code is used to analyze two systems in particular: Kepler-16 and CM Draconis. Magneto-convection is treated assuming stabilization of convection and also by assuming reductions in convective efficiency due to a turbulent dynamo. We find that magnetic stellar models are unable to reproduce the properties of inflated fully convective main-sequence stars, unless strong interior magnetic fields in excess of 10 MG are present. Validation of the magnetic field hypothesis given the current generation of magnetic stellar evolution models therefore depends critically on whether the generation and maintenance of strong interior magnetic fields is physically possible. An examination of this requirement is provided. Additionally, an analysis of previous studies invoking the influence of star spots is presented to assess the suggestion that star spots are inflating stars and biasing light curve analyses toward larger radii. From our analysis, we find that there is not yet sufficient evidence to definitively support the hypothesis that magnetic fields are responsible for the observed inflation among fully convective main-sequence stars in DEBs.

Key words: binaries: eclipsing – stars: evolution – stars: interiors – stars: low-mass – stars: magnetic field

Online-only material: color figures

1. INTRODUCTION

Outer layers of low-mass stars are unstable to thermal convection due to a rapid increase in opacity resulting from the partial ionization of hydrogen and the dissociation of H_2. Below $0.35\,M_\odot$, main-sequence stellar interiors are theorized to become fully convective along the main sequence (Limber 1958; Chabrier & Baraffe 1997). Largely characterized by near-adiabatic convection, fully convective stars are considered the simplest stars to describe from a theoretical perspective. In fact, properties of fully convective stars predicted by stellar structure models are largely insensitive to input variables (e.g., the mixing length parameter, α_{MLT}) and input physics (e.g., nuclear reaction rates, element diffusion; Chabrier & Baraffe 1997; Dotter et al. 2007). Discovery of significant radius discrepancies between observations and stellar model predictions for fully convective stars therefore presents a curious puzzle (see, e.g., Torres et al. 2010; Feiden & Chaboyer 2012a).

Evidence indicating that stellar structure models cannot properly predict radii of fully convective stars has been gathered from studies of detached eclipsing binaries (DEBs). Masses and radii can be measured for stars in DEBs with precisions below 3% provided the observations are of high quality and analyses are performed with care (Popper 1984; Andersen 1991; Torres et al. 2010). Presently, there are five DEBs with at least one fully convective component whose mass and radius has been quoted with precision below 3%: Kepler-38 (Orosz et al. 2012), Kepler-16 (Doyle et al. 2011; Winn et al. 2011; Bender et al. 2012), LSPM J1112+7626 (Irwin et al. 2011), KOI-126 (Carter et al. 2011), and CM Draconis (hereafter CM Dra; Lacy 1977; Metcalfe et al. 1996; Morales et al. 2009). Of these systems, only the fully convective stars of KOI-126 can be accurately characterized by stellar evolution models (Feiden et al. 2011; Spada & Demarque 2012). Every other fully convective star appears to have a radius inflated compared to model predictions.

Most consequential are the inflated radii of the stars in CM Dra. Historically, the stars of CM Dra are *the* fully convective stars against which to benchmark stellar models. As such, CM Dra has been well-studied and rigorously characterized. Over the years, discrepancies between model radii of CM Dra and those determined from observations has grown. Initial modeling efforts were optimistic that agreement could be achieved (Chabrier & Baraffe 1995), but disagreement was quickly identified with the introduction of more sophisticated models (Baraffe et al. 1998) and more precise mass and radius measurements (Metcalfe et al. 1996; Morales et al. 2009). This disparity has been increased, yet again, with converging reports of the system's metallicity (Rojas-Ayala et al. 2012; Terrien et al. 2012).

Strong magnetic fields maintained by tidal synchronization are presently considered the leading culprit producing the observed radius discrepancies (e.g., Mullan & MacDonald 2001; Ribas 2006; López-Morales 2007; Chabrier et al. 2007; Morales et al. 2008, 2009; MacDonald & Mullan 2012). Magnetic activity indicators, such as soft X-ray emission, Ca II H & K emission, and Hα emission, appear to correlate with radius inflation (López-Morales 2007; Feiden & Chaboyer 2012a; Stassun et al. 2012), providing evidence in favor of the magnetic hypothesis. Theoretical investigations also support a magnetic origin of radius inflation for main-sequence DEB stars (Chabrier et al. 2007; Morales et al. 2010; MacDonald & Mullan 2012; Feiden & Chaboyer 2013).

Despite significant evidence in favor of the magnetic hypothesis, several clues suggest otherwise. Discovery of the hierarchical triple KOI-126 in 2011 introduced a second pair of well-characterized fully convective stars whose masses and radii were measured with better than 2% precision. Stellar evolution models are able to reproduce the properties of KOI-126 (B, C), as previously mentioned, based only on inferred properties from the more massive primary star (Feiden et al. 2011;

Spada & Demarque 2012). With orbital and stellar properties similar to CM Dra, KOI-126 (B, C) presents a sharp contrast to known modeling disagreements.

Adding to the evidence mounting against the magnetic hypothesis, fully convective stars in Kepler-16, Kepler-38, and LSPM-J1112+7626 show inflated radii despite existing in long period (>17 days) systems. The fact that most inflated stars in DEBs appeared to exist in short period systems was proffered as strong circumstantial evidence in support of the magnetic hypothesis. However, only a few DEB systems were known, all of which had short orbital periods due to inherent observational biases. With the influx of data from long time baseline photometric monitoring campaigns, including *Kepler* and MEarth, fully convective stars in long period DEBs have been shown to have inflated radii.

Of course, the presence of inflated low-mass stars in long period systems is only contradictory if the inflated stars are slowly rotating ($v \sin i \lesssim 5$ km s^{-1}). Irwin et al. (2011) find that LSPM J1112+7626 A rotates with a period of 65 days, from which we infer an age of the order of 9 Gyr assuming the gyrochronology relation of Barnes (2010). This result requires confirmation, but if confirmed, it would be seem likely that the fully convective, low-mass secondary is slowly rotating. A rotation period has also been measured for the primary star in Kepler-16 (Winn et al. 2011). It was determined to be rotating with a period of nearly 36 days, close to the pseudo-synchronization rotation period (Hut 1981). If we assume the fully convective secondary has a similar rotation period (from pseudo-synchronization), then it would have $v \sin i < 0.5$ km s^{-1}, well below the empirical velocity threshold thought to be required for fully convective stars to maintain a strong magnetic field (Reiners et al. 2009). Therefore, in at least two cases, it appears that slowly rotating fully convective stars exhibit inflated radii.

In this paper, we extend our on-going investigation into the magnetic origin of inflated low-mass stellar radii, initiated in Feiden & Chaboyer (2012b, 2013), to fully convective stars. A brief overview of how we include magnetic effects in our models is presented in Section 2. Detailed analysis of two well-characterized DEBs, Kepler-16 and CM Dra, is given in Section 3 with a discussion of the results in Section 4. Section 4 also provides comparisons with previous studies and a careful examination of the magnetic hypothesis. A summary of key results and conclusions is then given in Section 5.

2. MAGNETIC DARTMOUTH STELLAR EVOLUTION CODE

Stellar evolution models used in this investigation are from the Dartmouth Magnetic Evolutionary Stellar Tracks and Relations (DMESTAR) program. DMESTAR was developed as an extension of the Dartmouth Stellar Evolution Program (DSEP; Dotter et al. 2008), a descendant of the Yale Rotating Evolution Code (Guenther et al. 1992). The magnetic version of the Dartmouth stellar evolution code is described in Feiden & Chaboyer (2012b), Feiden (2013), and Feiden & Chaboyer (2013). We refer the reader to these papers for a thorough overview.

2.1. Physics for Fully Convective Models

The pertinent aspects of the standard, non-magnetic stellar evolution code for modeling fully convective stars are the equation of state (EOS) and the surface boundary conditions. All fully convective stars are modeled with the FreeEOS, a publicly

available EOS code written by Alan Irwin and based on the free energy minimization technique.[3] We call FreeEOS in the EOS4 configuration to provide a balance between numerical accuracy and computation time. With this EOS, we are able to reliably model stars with masses above the hydrogen burning minimum mass (Irwin 2007).

Surface boundary conditions are prescribed using PHOENIX AMES-COND model atmospheres (Hauschildt et al. 1999). Atmosphere structures are used to define the initial gas pressure for our model envelope integration. Above 0.2 $M_\odot$, the gas pressure is determined an optical depth where $T = T_{\rm eff}$. However, below 0.2 $M_\odot$, the regime where convection is sufficiently non-adiabatic extends deeper into the star (Chabrier & Baraffe 1997). Thus, we specify our boundary conditions at the optical depth $\tau = 100$ in this mass regime. For the present work, we have extended the initial metallicity grid of model atmosphere structures (Dotter et al. 2007, 2008) by interpolating within the original set of structures. Care was taken to ensure that the interpolation produced reliable results and that no discontinuities in either $P_{\rm gas}$ or the starting temperature were introduced. This will be discussed in a future publication. A set of atmosphere structures with finer metallicity spacing allows for more accurate predictions of stellar properties at metallicities that lie between the original grid spacings.

2.2. Dynamos & Radial Profiles

Implementation of a magnetic perturbation is described in detail by Lydon & Sofia (1995) and Feiden & Chaboyer (2012b). We abstain from providing a mathematical description and refer the reader to those papers. However, it is beneficial to review multiple variations on our basic formulation that arose in Feiden & Chaboyer (2013). These variations take the form of different magnetic field strength radial profiles and what we have called different "dynamos." The latter refers not to a detailed dynamo treatment, but a conceptual framework that concerns from where we assume the magnetic field sources its energy.

2.2.1. "Rotational" versus "Turbulent" Dynamo

Our treatment of magneto-convection depends on how we assume the magnetic field is generated. Assuming that rotation drives the dynamo, as in a standard shell dynamo (Parker 1979), leads to perturbations consistent with the idea that magnetic fields can stabilize a fluid against thermal convection (e.g., Thompson 1951; Chandrasekhar 1961; Gough & Tayler 1966). This assumption forms the basis of our magneto-convection formulation (Feiden & Chaboyer 2012b, 2013). However, permissible magnetic field strengths can reach upward of 6 kG at the model photosphere with exact upper limits determined by equipartition with the thermal gas pressure. This also results in interior magnetic field strengths that can grow nearly without limit owing to large internal gas pressures. Models that rely on stabilizing convection with a magnetic field are hereafter referred to as having "rotational dynamos."

The form of the perturbation used for a star with an assumed rotational dynamo is not necessarily valid in all stellar mass regimes. This is particularly true in fully convective stars, where the interface region between the radiative core and convective envelope is thought to disappear. To address this, and the problem that magnetic fields in the rotational dynamo can grow without limit, we introduced a "turbulent dynamo" mechanism (Feiden & Chaboyer 2013). This formulation assumes that

---

[3] Available at http://www.freeeos.sourceforge.net/.

the magnetic field strength at a given grid point within the model receives its energy from the kinetic energy of convecting material. Therefore, the local Alfvén velocity cannot exceed the local convective velocity. It is a simple approach developed to address zeroth-order effects within the already simplified convection framework of mixing length theory. For low-mass stars, this methods places an upper limit of around 3 kG for surface magnetic field strengths, consistent with observed upper limits of average surface magnetic field strengths (Reiners & Basri 2007; Shulyak et al. 2011). Although rotation is still required for turbulent dynamo action (Durney et al. 1993; Dobler et al. 2006; Chabrier & Küker 2006; Browning 2008), magnetic field strengths are more sensitive to properties of convection.

We note, again, that the term "dynamo" is used loosely. Our formulations of magneto-convection do not rigorously solve the equations of magnetohydrodynamics. Instead, we seek to capture physically relevant effects on stellar structure in a phenomenological manner consistent with actual dynamo processes. Each of the above descriptions rely equally on a prescribed magnetic field strength profile within the star.

2.2.2. Dipole Radial Profile

Models of the "dipole radial field" variety are the standard sort introduced in Feiden & Chaboyer (2012b). This profile is characteristic of a magnetic field generated by a single current loop centered on the stellar tachocline. Given a surface magnetic field strength, the radial profile of the magnetic field is determined by calculating the peak magnetic field strength at the tachocline. Lacking a tachocline, we define fully convective stars to have a peak magnetic field strength at 15% of the stellar radius ($0.15 R_\star$). This is loosely based on results from three-dimensional (3D) magnetohydrodynamic (MHD) models of fully convective stars (Browning 2008). MHD models indicate that the magnetic field reaches a maximum around $\sim 0.15\,R_\star$ (Browning 2008). Note that this maximum is not a sharply defined peak in the magnetic field strength profile since the profile is based largely on equipartition of the magnetic field with convective flows. Still, we adopt $0.15\,R_\star$ knowing this caveat, which we address in a moment. The rest of the interior magnetic field is then calculated by assuming the magnetic field strength falls off steeply toward the core and surface of the star. Explicitly,

$$B(R) = B_{\mathrm{surf}} \cdot \begin{cases} R^3/R_{\mathrm{tach}}^6 & R < R_{\mathrm{tach}} \\ R^{-3} & R > R_{\mathrm{tach}} \end{cases}, \qquad (1)$$

where B_{surf} is the prescribed surface magnetic field strength, R_{tach} is the radius of the tachocline normalized to the total stellar radius, and R is the radius within the star normalized to the total stellar radius.

2.2.3. Gaussian Radial Profile

To increase the peak magnetic field strength for a given surface magnetic field strength, we implemented a Gaussian profile (Section 4.4.1 in Feiden & Chaboyer 2013). The peak magnetic field strength is still defined at the tachocline in partially convective stars and at $R = 0.15\,R_\star$ in fully convective stars. However, instead of a power-law decline of the interior magnetic field strength from the peak, the peak was set as the center of a Gaussian distribution. Thus,

$$B(R) = B(R_{\mathrm{tach}}) \exp\left[-\frac{1}{2}\left(\frac{R_{\mathrm{tach}} - R}{\sigma_g} \right)^2 \right], \qquad (2)$$

where σ_g controls the width of the Gaussian and $B(R_{\mathrm{tach}})$ is defined with respect to the surface magnetic field strength. The width of the Gaussian depends on the depth of the convection zone. Deeper convection zones have a wider Gaussian profile compared to stars with thin convective envelopes (Feiden & Chaboyer 2013). Hereafter, we will refer to these as "Gaussian radial profile" models. Note that this prescription has no physical motivation beyond providing stronger interior magnetic fields.

2.2.4. Constant Λ Radial Profile

We define a third radial profile for this study: a "constant Λ radial profile." When a turbulent dynamo is invoked, the magnetic field radial profiles described above can cause the Alfvén velocity to exceed the convective velocity within the model interior. This happens quite easily in models of fully convective stars where the peak magnetic field strength is defined deep within the model. As a result, perturbed convective velocities become imaginary leading convergence problems when solving the equations of mixing length theory.

If we assume that kinetic energy in convective flows generates the local magnetic field, an Alfvén velocity exceeding the convective velocity will lead to a decaying magnetic field strength. Eventually, equipartition will be reached. We avoid iterating to a solution by using a profile that assumes a constant ratio of magnetic field to the equipartition value, $B(r) = \Lambda B_{\mathrm{eq}}$, where $B_{\mathrm{eq}} = (4\pi\rho u_{\mathrm{conv}}^2)^{1/2}$. This factor, Λ, was introduced in Feiden & Chaboyer (2013) as a means of comparing reduced mixing length models (i.e., Chabrier et al. 2007) to our turbulent dynamo models.

Perturbations to the equations of mixing length theory are now expressed as functions of Λ. Removing energy from convection slows convective flows such that

$$u_{\mathrm{conv}} = u_{\mathrm{conv},0}(1 - \Lambda^2)^{1/2}, \qquad (3)$$

where $u_{\mathrm{conv},0}$ is the convective velocity prior to losing energy to the magnetic field. We restrict $0 \leqslant \Lambda \leqslant 1$ to avoid imaginary convective velocities. Reduction of convective velocity causes a significant reduction in convective energy flux since $\mathcal{F} \propto u_{\mathrm{conv}}^3$. Steeping of the background temperature gradient, ∇_s, occurs as radiation attempts to transport additional energy. This increase, $\Delta\nabla_s$, over the non-perturbed temperature gradient is

$$\Delta\nabla_s = \frac{(\Lambda u_{\mathrm{conv}0})^2}{C}, \qquad (4)$$

where $C = g\alpha_{\mathrm{MLT}}^2 H_P \delta/8$ is the characteristic squared velocity of an unimpeded convecting bubble over a pressure scale height. This is a sort of terminal convective velocity, where g is the local acceleration due to gravity, α_{MLT} is the convective mixing length parameter, H_P is the pressure scale height, and $\delta = (\partial \ln \rho/\partial \ln T)_{P,\chi}$ is the coefficient of thermal expansion. Resulting effects on convection likely represent an upper limit on the effects of such a dynamo mechanism in inhibiting thermal convection. Note that when using this radial profile and dynamo mechanism, modifications to the Schwarzschild criterion (i.e., the formalism outlined in Feiden & Chaboyer 2012b) are neglected.

3. ANALYSIS OF INDIVIDUAL DEB SYSTEMS

We have chosen to study the DEBs Kepler-16 and CM Dra in detail. LSPM J1112+7626 was not modeled in detail because it lacks a proper metallicity estimate required for a careful
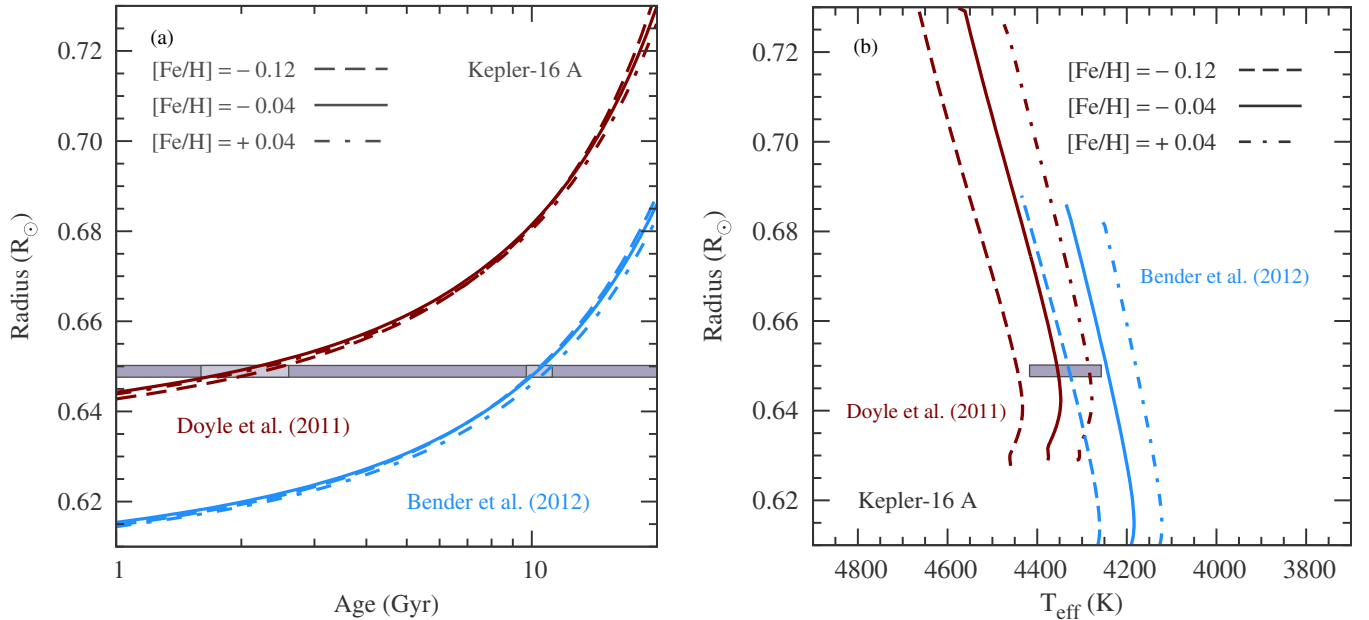
Figure 1. Standard Dartmouth models computed at the exact masses measured by Doyle et al. (2011; maroon) and Bender et al. (2012; light-blue) for Kepler-16 A. Mass tracks for the adopted metallicity of Winn et al. (2011) and the two limits of the associated 1σ uncertainty are given by solid, dashed, and dashed-dotted lines, respectively. (a) Age–radius diagram with the observed radius indicated by the purple horizontal swath. (b) $T_{\rm eff}$–radius plane where the purple box indicates observational constraints for Kepler-16 A.

(A color version of this figure is available in the online journal.)

Table 1
Fundamental Properties of Kepler-16

Property	Kepler-16 A	Kepler-16 B
D11 Mass ($M_\odot$)	0.6897 ± 0.0034	0.20255 ± 0.00066
B12 Mass ($M_\odot$)	0.654 ± 0.017	0.1959 ± 0.0031
Radius ($R_\odot$)	0.6489 ± 0.0013	0.2262 ± 0.0005
$T_{\rm eff}$ (K)	4337 ± 80	. . .
[Fe/H]		-0.04 ± 0.08
Age (Gyr)		3 ± 1

comparison with models. Kepler-38 was also not selected as initial comparisons suggest that there may be some issues with modeling the primary. Finally, KOI-126 has been modeled in detail previously and does not appear to require magnetic fields (Feiden et al. 2011; Spada & Demarque 2012). As we will show below, magnetic models of Kepler-16 B and CM Dra produce similar results that can be generalized to all fully convective main-sequence stars in DEBs.

3.1. Kepler-16

Report of the first circumbinary exoplanet was announced by Doyle et al. (2011) with their study of Kepler-16b. While the planet is interesting in its own right, what made the finding even more interesting was that the two host stars formed a long-period low-mass DEB. This enabled a precise characterization of the stars and circumstellar environment. Kepler-16 contains a K-dwarf primary with a fully convective M-dwarf secondary in a 41 day orbit. Properties of the two stars are listed in Table 1.

In a follow-up investigation, Winn et al. (2011) estimated the composition and age of the system. An age of 3 ± 1 Gyr was estimated using gyrochronology and an age-activity relation based on Ca II emission. Spectroscopic analysis of the primary revealed the system has a solar-like metallicity of [Fe/H] = -0.04 ± 0.08 dex. They also compared properties of the

Kepler-16 stars to predictions of stellar evolution models. Baraffe et al. (1998) model predictions agreed with properties of the primary at the given age. However, the radius of the fully convective secondary star was larger than model predictions by ∼3%. Independent confirmation of the stellar properties and model disagreements was provided by Feiden & Chaboyer (2012a), who found a best-fit age of 1 Gyr with [Fe/H] = -0.1 using Dartmouth models.

Radial velocity confirmation of the component masses—within 2σ—was later obtained by Bender et al. (2012). They found masses that were 5% lower than the original masses (Doyle et al. 2011). Of particular note, is that mass ratio is different between the two studies. Bender et al. (2012) attempted to pin-point the origin of this discrepancy, but were unable to do so with complete confidence.

Despite the disagreement, the spectroscopic masses largely confirm that masses derived using a photometric-dynamical model are reliable (Carter et al. 2011; Doyle et al. 2011). However, a slight mass difference significantly alters comparisons with stellar evolution models. That is, if we assume that the derived masses do not heavily influence the radius and effective temperature predictions. We therefore opt to treat the two different mass estimates independently to assess how these differences affect our modeling efforts. Hereafter, masses originally quoted by Doyle et al. (2011) will be referred to as D11 masses, whereas the revised values of Bender et al. (2012) will be referred to as B12 masses. Table 1 lists masses measured by each group.

3.1.1. Standard Models

We first focus our attention on Kepler-16 A, as the analysis will directly influence our analysis of the secondary. Plotted in Figure 1 are non-magnetic Dartmouth models computed at the measured masses of the primary provided by D11 and B12. Three separate tracks are illustrated for each mass

estimate, corresponding to [Fe/H] = −0.12, −0.04, and +0.04 (Winn et al. 2011). In this figure, the horizontal shaded region highlights the observed radius with associated 1σ uncertainties. Ages are determined by noting where the mass tracks are located within the bounds of the empirical radius constraints. Similarly, we confirm that when the mass track has the required radius it also has an appropriate effective temperature in Figure 1(b).

Given a primary mass from D11, we find that standard stellar evolution models match the stellar radius and temperature at an age of 2.1 ± 0.5 Gyr. When the model radius equals the precise empirical radius ($0.6489\ R_\odot$), the associated model effective temperature is 4354 K, which is within 17 K of the spectroscopic effective temperature (Winn et al. 2011). We note that this age is also consistent with the estimated age from Winn et al. (2011).

Agreement between models and observations does not guarantee the validity of the D11 masses over the B12 masses. In fact, this agreement is rather expected. The effective temperature and metallicity for the primary were determined using Spectroscopy Made Easy (hereafter SME; Valenti & Piskunov 1996), which relies on theoretical stellar atmospheres. Our models also rely on theoretical atmospheres, although PHOENIX model atmospheres, used by our models, adopt a different line list database (see Hauschildt et al. 1999 and references therein) than the theoretical atmospheres used by SME (VALD: Vienna Atomic Line Database; Piskunov et al. 1995). In a sense, the fact that we find such good agreement with the effective temperature for a given log g and metallicity (i.e., those of Kepler-16 A) may be a better test of the agreement between different stellar atmosphere models rather than a test of the interior evolution models. What is encouraging, is that we derive appropriate stellar properties at an age consistent with gyrochronology and age-activity relations Winn et al. (2011). Age consistency is not ensured by agreement between stellar atmosphere structures.

Our previous discussion may be erroneous if we adopt an incorrect mass. B12 suggest this is the case. The effect of adopting the lower B12 masses is displayed in Figure 1. Assuming the radius measurement remains constant, we derive an age of 10.5 ± 0.8 Gyr for the primary star. The effective temperature associated with the model also appears too cool compared to observations at the measured metallicity (−0.04 dex). Relief is found by lowering the metallicity by 0.1 dex, which increases the temperature by 30 K. This is enough to bring the model temperature to within 1σ of the spectroscopic value (Winn et al. 2011).

There is a caveat: the spectroscopic analysis by Winn et al. (2011) relied on fixing the stellar log g as input into SME. Thus, the temperature and metallicity are intimately tied to the adopted log g. Reducing the mass of the primary by 5%, as is done by B12, but leaving the radius fixed to the D11 value leads to a decrease in log g of 0.02 dex. Such a change in the fixed value of log g may decrease the derived effective temperature and bring the model and empirical temperatures into agreement. All things considered, we believe it is safe to assume that a shift in mass does not introduce any significant effective temperature disagreements at a given radius. This is predicated on the fact that the temperature is safely above ∼4000 K. Below this temperature, theoretical atmosphere predictions start to degrade with the appearance of molecular bands. More simply stated, we have no reason to doubt the Dartmouth model predicted temperature for Kepler-16 A, regardless of the adopted mass.

A model age of 11 Gyr for the B12 primary mass appears old given the multiple age estimates provided by Winn et al. (2011). Is it possible that the system is actually 11 Gyr old, but
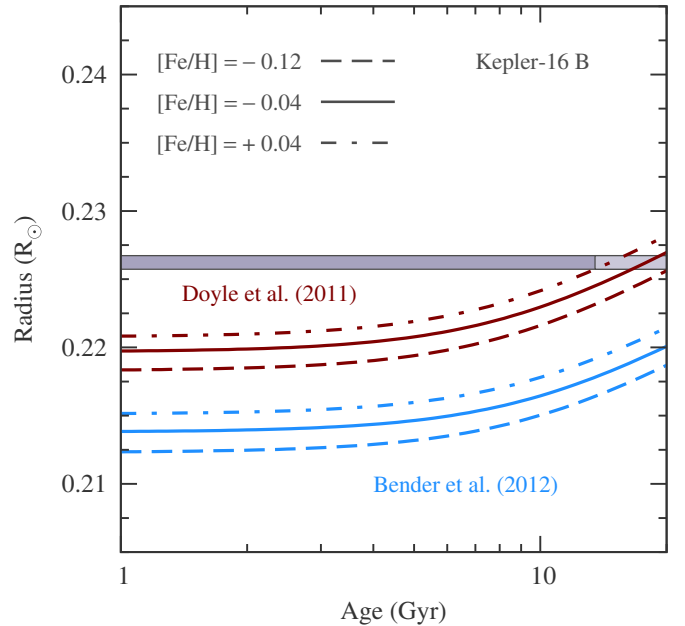

Figure 2. Identical to Figure 1(a), except the mass tracks are computed at the masses measured for Kepler-16 B.

(A color version of this figure is available in the online journal.)

appears from rotation and activity to be considerably younger? Consider that a 35.1 ± 1.0 day rotation period of the primary, as measured by Winn et al. (2011), is nearly equal to the pseudo-synchronization rotation period, predicted to be 35.6 days (Hut 1981; Winn et al. 2011). One might think that tidal effects are unimportant in a binary with a 41 day orbital period, however, subsequent tidal interactions briefly endured when the components are near periastron can drive the components toward pseudo-synchronous rotation. Pseudo-synchronous rotation will keep the stars rotating at a faster rate than if they were completely isolated from one another. The timescale for this to occur is approximately 3 Gyr (Winn et al. 2011), meaning that the rotation period is not necessarily indicative of the system's age. The primary will have approximately the same rotation period at 11 Gyr as it will at 3 Gyr. Furthermore, the timescale for orbital circularization is safely estimated to be between ∼10^4 and 10^5 Gyr (Winn et al. 2011). Tidal evolution calculations are subject to large uncertainties and should approached as an order of magnitude estimate. However, we are unable to immediately rule out the possibility that Kepler-16 has an age of 11 Gyr.

We have so far neglected any remark on the agreement between standard models and Kepler-16 B. This comparison is carried out in Figure 2. No effective temperature estimates have been published, explaining our neglect of the $T_{\rm eff}$–radius plane. As with Figure 1, mass tracks are shown for multiple metallicities. Standard model mass tracks for Kepler-16 B are unable to correctly predict the observed radius at an age consistent with estimates from the primary. The disagreement is independent of the adopted metallicity, which introduces ∼0.5% variations in the stellar radius at a given age.

No evidence is available to support the idea that Kepler-16 B is magnetically active. Still, we look to magnetic fields to reconcile the model predictions with the observations. All possible scenarios relating to the various stellar mass estimates are considered. Explicitly, we compute models for both the D11 and B12 masses and then attempt to fit the observations using the magnetic Dartmouth stellar evolution models.
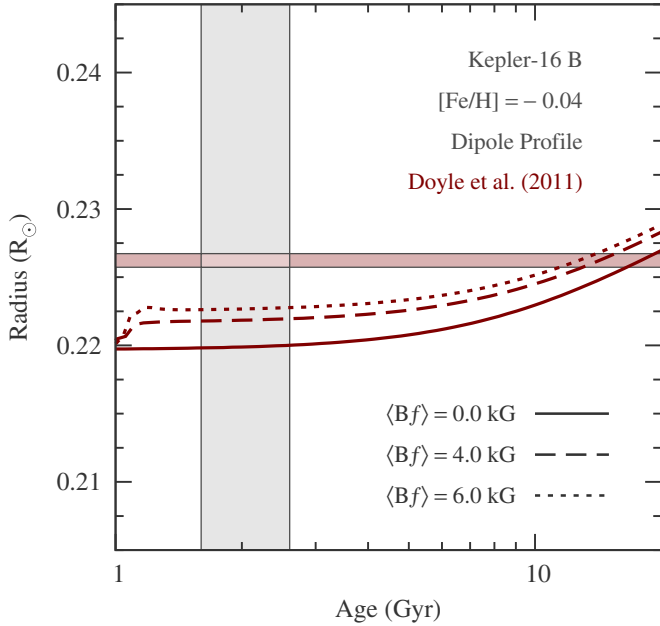
Figure 3. Standard (solid line) and magnetic (broken lines) Dartmouth models of Kepler-16 B with a D11 mass. Models were computed with [Fe/H] = −0.04 and a solar calibrated $\alpha_{\rm MLT}$. Magnetic models were calculated using a dipole radial profile with a 4.0 kG (dashed line) and a 6.0 kG (dotted line) surface magnetic field strength. Observed radius constraints are shown as a shaded horizontal region and an age constraint is given by the vertical shaded region.

(A color version of this figure is available in the online journal.)

3.1.2. Magnetic Models: D11 Masses

The D11 primary mass implies that Kepler-16 is approximately 2 Gyr old, as shown in Figure 1(a). Due to the consistency between the model derived age and the empirically inferred age, we see no reason to introduce a magnetic perturbation into models of Kepler-16 A. Winn et al. (2011) observe only moderately weak chromospheric activity coming from the primary, further supporting our decision. Thus, we seek to reconcile models of Kepler-16 B with D11 masses at 2 Gyr.

Magnetic models of Kepler-16 B were computed for a range of surface magnetic field strengths. A dipole radial profile was used and the perturbation was applied over a single time step at an age of 1 Gyr. Mass tracks with a 4.0 kG and 6.0 kG surface magnetic field strength are shown in Figure 3 alongside a standard mass track for comparison. Note, that even though the perturbation is applied at an age close to the age we are trying to fit, the models adjust to the perturbation rapidly. We are unable to produce a radius inflation larger than 1%, even with a strong surface magnetic field strength of 6.0 kG. The peak field strength in the 6.0 kG model (located at $R = 0.15\,R_\star$) is approximately 1.8 MG ($\nu \approx P_{\rm mag}/P_{\rm gas} = 10^{-6}$). Discussion about how real such a magnetic field might be is deferred until Section 4.3.2. For the moment, we are interested in knowing what magnetic field strength is required to reconcile models with observations.

We next constructed magnetic models using a Gaussian radial profile, which are shown in Figure 4. The magnetic perturbation was again introduced as a single perturbation at 1 Gyr. Two surface magnetic field strengths were used, 4.0 kG and 5.0 kG. The model with a 5.0 kG surface magnetic field strength causes the model to become over inflated compared to the observed radius at 2 Gyr. From Figure 4, we see that a magnetic field intermediate between 4 kG and 5 kG is required to produce agreement between the models and observations. In contrast to
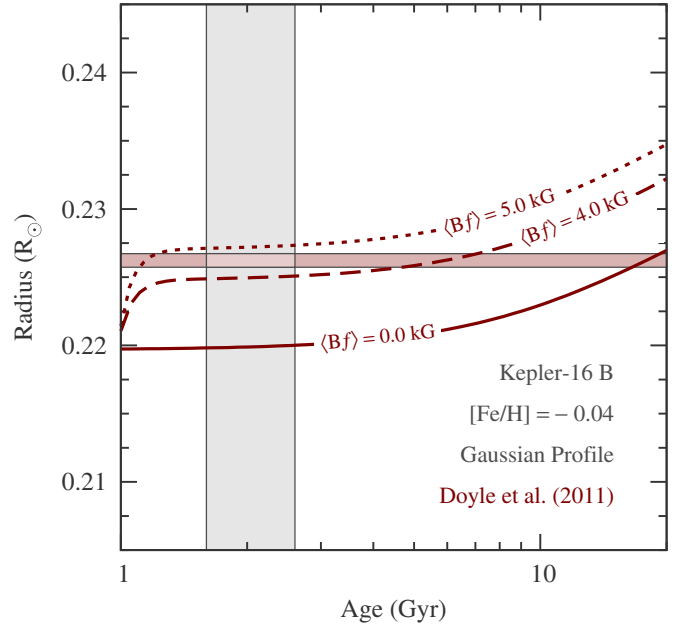

Figure 4. Same as Figure 3, except the magnetic models were computed with a Gaussian radial profile.

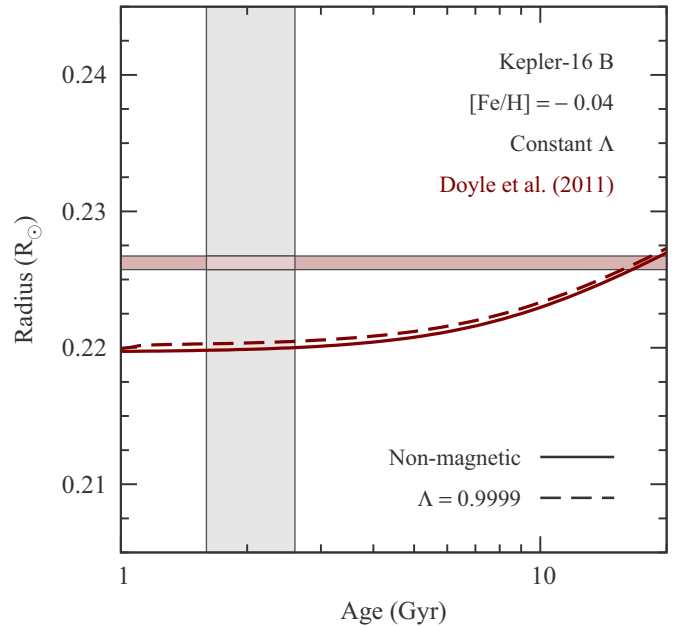(A color version of this figure is available in the online journal.)

Figure 5. Same as Figure 3, but the magnetic model was calculated using a constant $\Lambda = 0.9999$ profile.

(A color version of this figure is available in the online journal.)

results for partially convective stars (Feiden & Chaboyer 2013), dipole and Gaussian radial profiles produce different results for a given surface magnetic field strength in fully convective stars. This is caused by a difference in peak magnetic field strengths (dipole: 1.8 MG, $\nu = 10^{-6}$; Gaussian: 30 MG, $\nu = 10^{-4}$). We will return to this issue in Section 4.1.

Finally, Figure 5 shows the influence of a constant Λ profile on a model of Kepler-16 B. Recall, this radial profile invokes a turbulent dynamo mechanism. We started with a rather high value of $\Lambda = 0.9999$ to gauge the model's reaction to this formulation. Impact on the radius evolution of a $M = 0.203\,M_\odot$
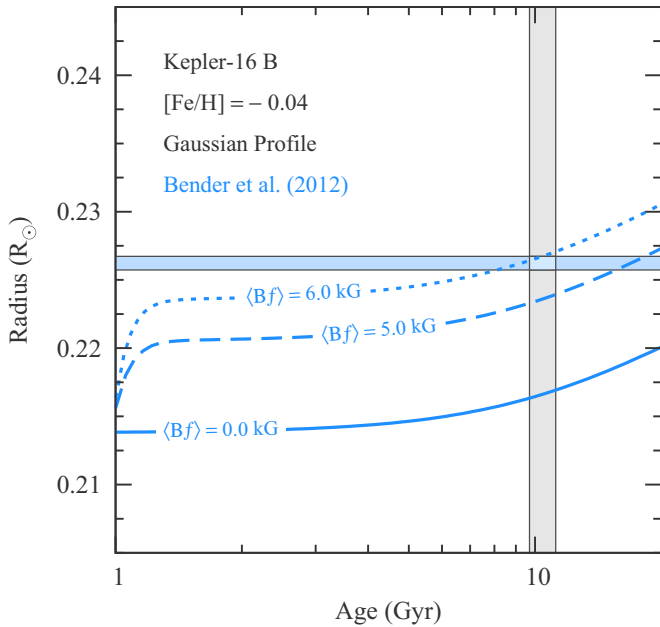
Figure 6. Similar to Figure 4, but with B12 masses and a Gaussian radial profile. Surface magnetic field strengths used were 5.0 kG (dotted line) and 6.0 kG (dashed-dotted line).

(A color version of this figure is available in the online journal.)

star is effectively negligible. Further increasing Λ has no effect on the resulting radius evolution.

3.1.3. Magnetic Models: B12 Masses

Adopting B12 masses mainly alters the age derived from stellar models. Instead of 2 Gyr, we infer an age of 11 Gyr from models of Kepler-16 A, as was shown in Figure 1(a). The relative radius discrepancy noted between models and Kepler-16 B is increased by approximately 2% over the D11 case.

Magnetic models were computed for Kepler-16 B with the B12 mass estimate using a Gaussian radial profile introduced at an age of 1 Gyr. These models are shown in Figure 6. We did not generate models with a dipole radial profile or with a constant Λ profile given the lack of radius inflation observed for these magnetic field profiles for the D11 masses. We find that a surface magnetic field strength slightly weaker than 6.0 kG is required to fit the observations. This translates to a nearly 40 MG ($\nu = 10^{-4}$) peak magnetic field strength. A stronger field strength was required when using the B12 mass instead of the D11 mass because of the 1% increase in the radius discrepancy mentioned above.

3.1.4. Summary

Kepler-16, although it has components with fundamental properties measured with better than 3% precision, must be approached cautiously when comparing to stellar models. Mass differences quoted in the literature obscure how well models perform against the observations. Though the masses are determined with high precision by each group, the 3%–5% uncertainty introduced by their disagreement overwhelms the measurement precision. This produces an age difference of 9 Gyr for the primary star, calling into question inferences drawn about this system from stellar models. It is also unclear how revising the masses would affect estimates of the component radii, the system's metallicity, and the primary star's effective temperature. Furthermore, since the primary may be rotating pseudo-

Table 2
Fundamental Properties of CM Draconis

Property	CM Dra A	CM Dra B
Mass ($M_\odot$)	0.23102 ± 0.00089	0.21409 ± 0.00083
Radius ($R_\odot$)	0.2534 ± 0.0019	0.2398 ± 0.0018
$T_{\rm eff}$ (K)	3130 ± 70	3120 ± 70
[Fe/H]	-0.30 ± 0.12	
Age (Gyr)	4.1 ± 0.8	

synchronously, it is not possible to rule out either of the age estimates.

Until the mass differences are resolved, *care must be taken when comparing Kepler-16 to stellar models*. However, the disparity between the observed radius of Kepler-16 B and model predictions is apparent regardless of the adopted mass estimate. Changing the mass estimate simply changes the level of inferred radius inflation. This result appears robust and can be used to test the magnetic hypothesis for low-mass star radius inflation. Our magnetic models require magnetic field strengths of similar magnitudes. Surface magnetic field strengths are on the order of 4 kG–6 kG with interior field strengths of a few tens of MG.

3.2. CM Draconis

CM Dra (GJ 630.1 AC) contains two fully convective low-mass stars and is arguably one of the most important systems for benchmarking stellar evolution models. Shortly after CM Dra was discovered by Luyten, Eggen & Sandage (1967) uncovered that the star was actually a DEB. It was not clear from observations whether the secondary was a dark, very low-mass companion such that no secondary eclipse occurred or whether the two components were of nearly equal mass. Evidence was tentatively provided in favor CM Dra being a single dMe star with a dark companion (Martins 1975), although more observations were encouraged as the author found a possible hint of a secondary eclipse. Any speculation that the secondary companion to the dMe star of CM Dra was a dark, lower-mass object was laid to rest by Lacy (1977) who obtained radial velocity measurements to provide the first determination of stellar parameters for both stars.

Following Lacy's determination of the stellar properties, subsequent studies refined and improved the masses and radii of the CM Dra stars, pushing the measurement precision below 2% (Metcalfe et al. 1996; Morales et al. 2009). Currently accepted values (Morales et al. 2009; Torres et al. 2010) are listed in Table 2. Additional information about the CM Dra stars has been revealed in recent years. Morales et al. (2009) provided an analysis of a nearby white dwarf (WD 1633+572) common proper motion companion and estimated an age of 4.1 ± 0.8 Gyr. This age was based upon the cooling time of the white dwarf and its estimated progenitor lifetime, which depends on the initial to final mass relation for white dwarfs. In light of recent advances in our understanding of white dwarf cooling (e.g., Salaris et al. 2010) and the initial-to-final mass relation (e.g., Kalirai et al. 2009), we intend to re-examine the question of the age of CM Dra in a future paper. For the present work, we adopt the aforementioned age.

Deriving a metallicity for CM Dra has proven more difficult than estimating its age. Near-infrared (NIR) spectroscopic studies that fit theoretical model atmospheres to atomic and molecular features have consistently favored a metal-poor abundance ([M/H] ≈ -0.6; Viti et al. 1997, 2002; Kuznetsov et al. 2012). Optical spectroscopy of molecular features (CaH & TiO;
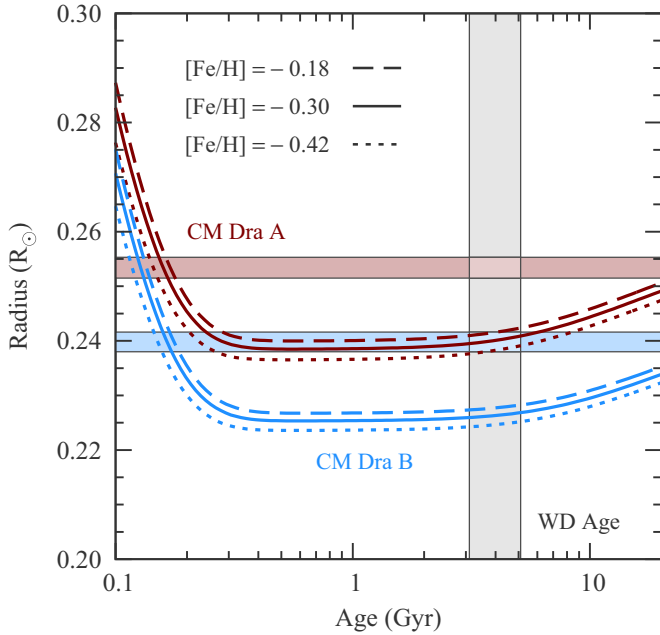
Figure 7. Standard Dartmouth models of CM Dra A (maroon) and B (light-blue). Models were computed with [Fe/H] = −0.18 (dashed line), −0.30 (solid line), and −0.42 (dotted line) and a solar calibrated α_{MLT}. Observed radius constraints are shown as shaded horizontal regions and an age constraint is given by a vertical shaded region.

(A color version of this figure is available in the online journal.)

Figure 8. Standard (solid line) and magnetic (dashed line) Dartmouth models of CM Dra A (maroon) and B (light-blue). Models were computed with [Fe/H] = −0.18 and a solar calibrated α_{MLT}. (Top) Magnetic models with a dipole radial profile and a 5.0 kG surface magnetic field strength. (Bottom) Magnetic models with a Gaussian radial profile and a 6.0 kG surface magnetic field strength. Observed radius constraints are shown as shaded horizontal regions (color-matched to the mass tracks) and an age constraint is given by a vertical shaded region.

(A color version of this figure is available in the online journal.)

Gizis 1997) and NIR photometric colors (Leggett et al. 1998), on the other hand, suggests that the system might have a near-solar metallicity. More recent techniques relying on empirically-calibrated narrow-band NIR (H & K band) spectral features have converged on a value of [M/H] = −0.3 ± 0.1 (Rojas-Ayala et al. 2012; Terrien et al. 2012). Further support for the latter estimate is provided by the photometric color-magnitude-metallicity relation of Johnson & Apps (2009), which predicts [Fe/H] ≈ −0.4. For this study, we adopt [Fe/H] = −0.30 ± 0.12 presented by Terrien et al. (2012) who controlled for uncertainties introduced by orbital phase variations.

It is well documented that the stars of CM Dra are inflated compared to standard stellar models (Ribas 2006; Morales et al. 2009; Torres et al. 2010; Feiden & Chaboyer 2012a; Spada & Demarque 2012; Terrien et al. 2012). This fact has become steadily more apparent since an initial comparison was performed by Chabrier & Baraffe (1995), which found little disagreement. A precise estimate of the level of disagreement depends on the adopted metallicity (see, e.g., Feiden & Chaboyer 2012a; Terrien et al. 2012), but the problem is robust. Figure 7 demonstrates the level of disagreement compared to standard Dartmouth mass tracks. It also illustrates how metallicity influences the stellar models. Given that there is no evidence for polar spots on CM Dra (see Section 4.3.3), we have elected to use the radii established by Torres et al. (2010). The level of disagreement observed in Figure 7 is between 5% and 7% for each star, with CM Dra A have a consistently smaller deviation than CM Dra B by about 0.5%. Terrien et al. (2012), as a consequence of their metallicity estimate, have essentially doubled the radius disagreement from 3% to 4%, noted in previous studies (e.g., Feiden & Chaboyer 2012a), to 5%–7%.

CM Dra is magnetically active. Balmer emission and light curve modulation due to spots have been recognized since very early investigations (Zwicky 1966; Martins 1975; Lacy 1977).
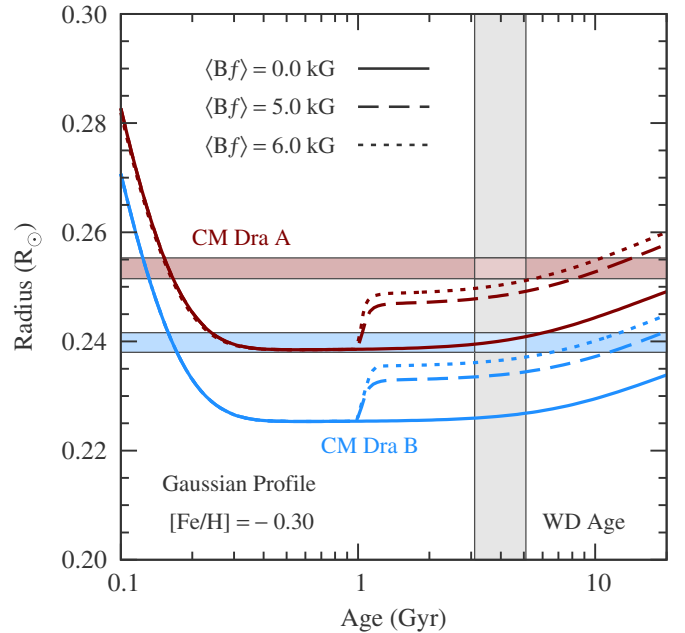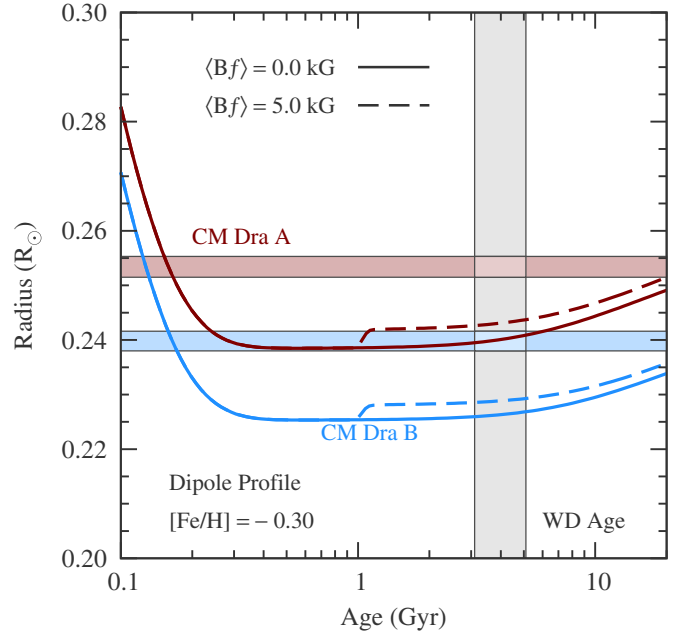
Frequent optical flaring has also been continually noted (e.g., Eggen & Sandage 1967; Lacy 1977). Further details on the flare characteristics of CM Dra may be found in the work by MacDonald & Mullan (2012). The system is also a strong source of X-ray emission based on an analysis of data in the ROSAT All-Sky Survey Bright Source Catalogue (Voges et al. 1999; López-Morales 2007; Feiden & Chaboyer 2012a).

High levels of magnetic activity and a short orbital period (1.27 days) have been used to justify the need for magnetic
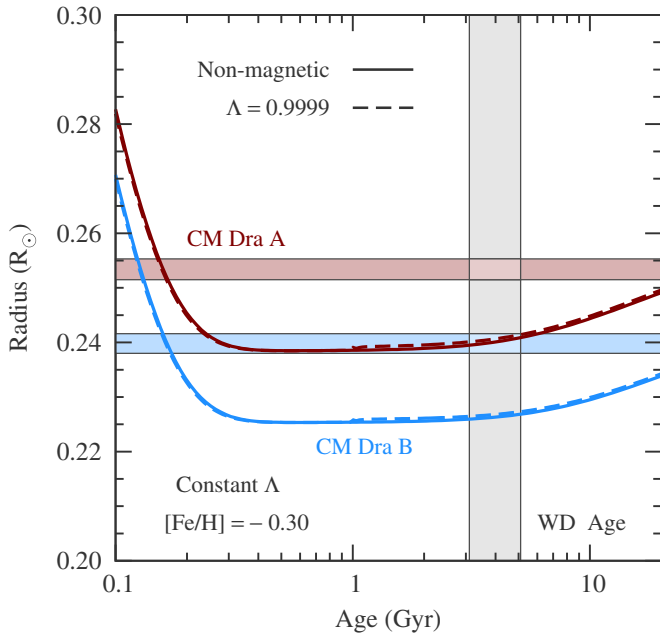
Figure 9. Same as Figures 8(a) and (b), but the magnetic model was calculated with a constant $\Lambda = 0.9999$ turbulent dynamo formulation.

(A color version of this figure is available in the online journal.)

Figure 10. Difference between the real temperature gradient, ∇_s, and the adiabatic temperature gradient, ∇_{ad}, as a function of the logarithmic plasma density for a $M = 0.231\ M_\odot$ star. We show this for two models: a non-magnetic model (maroon, solid line) and a magnetic model (light-blue, solid). The zero point is marked by a gray dashed line, dividing locations where convection (positive) or radiation (negative) is the dominant flux transport mechanism. The inset zooms in on the deep interior where the magnetic field creates a small radiative core.

(A color version of this figure is available in the online journal.)

perturbations in stellar evolution models of CM Dra. Such studies were carried out by Chabrier et al. (2007), Morales et al. (2010), and MacDonald & Mullan (2012) using various methods (see Section 4.3 of this work). In each case, magnetic models were found to provide satisfactory agreement with the observations. CM Dra therefore provides a pivotal test of our models and of the magnetic field hypothesis.

Magnetic model mass tracks are displayed in Figures 8 and 9. We computed magnetic models using all three radial profiles discussed in Section 2.2 and using both dynamo formulations. Perturbations were introduced over a single time step at an age of 1 Gyr. As with Kepler-16 B, the magnetic models adjust to the perturbation well before the age where we attempt to perform the fit of models to observations. All magnetic models have [Fe/H] = −0.30 and a solar-calibrated α_{MLT}. Since model radius predictions are only affected at the 1% level due to metallicity variations, inflation required of magnetic fields is the dominating factor when attempting to correct radius deviations of 6%.

Results for CM Dra are similar to those for Kepler-16 B. Models with a dipole radial profile are unable to inflate model radii at the level needed, despite strong surface magnetic field strengths being applied (5.0 kG–6.0 kG). This is evidenced in Figure 8(a), where magnetic-field-induced inflation occurs at the 1%–2% level. Gaussian radial profile models were able to largely reconcile models with observations. Figure 8(b) shows that surface magnetic field strengths of ∼6.0 kG are required to provide the necessary radius inflation. Note that in 8(b) the 6.0 kG mass track for CM Dra A actually has a 5.7 kG magnetic field for reasons related to model convergence. One can also see in Figure 8(b) that CM Dra B requires a slightly stronger magnetic field strength. As with Kepler-16 B, the peak interior magnetic field strengths are 1.8 MG ($\nu = 10^{-6}$) and 40 MG ($\nu = 10^{-4}$) for the dipole and Gaussian profiles, respectively. Constant Λ models are shown in Figure 9. We only plot a $\Lambda = 0.9999$ for each mass. Model radius inflation induced by these models is negligible, as with the case for Kepler-16 B.
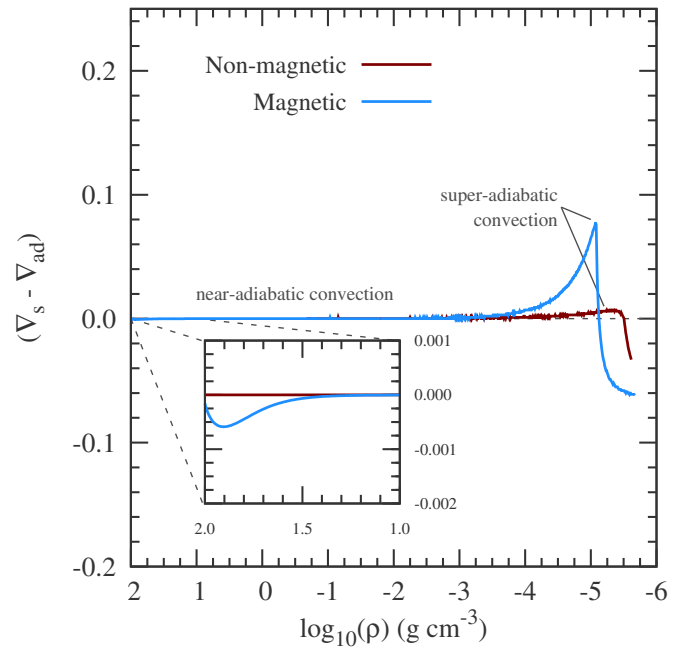
4. DISCUSSION

4.1. Magnetic Field Radial Profiles

The different results produced by the three magnetic field profiles introduced in Section 2.2 can be understood in terms of convective efficiency (Spruit & Weiss 1986; Feiden & Chaboyer 2013). Convection near the surface of partially convective stars displays a higher level of super-adiabaticity than does convection in the outer layers of fully convective stars. In general, this suggests that convection is less efficient in the outer layers of partially convective stars. The structure of partially convective stars is therefore more sensitive to changes in convective properties. As a result, structural changes induced by modification to convective properties at the stellar surface induce the necessary radius inflation before the interior magnetic field strength becomes large enough to inhibit convection near the base of the convection zone. Dipole and Gaussian profiles then produce similar results for partially convective stars.

For fully convective stars, the situation is reversed. We display the run of ($\nabla_s - \nabla_{ad}$) in two models of CM Dra A in Figure 10. One standard Dartmouth model and one magnetic model are shown. The magnetic model is a Gaussian radial profile model with a 6.0 kG surface magnetic field. This is the same model that was plotted in Figure 8(b). Fully convective stars are largely characterized by near-adiabatic convection from the outer layers down to the core of the star. Changes in convective properties have little effect on the flux transported by convection because convection is extremely efficient. Changes to the properties of convection do have some structural effects (see Figure 8(a)), but they are minimal. It is not until the deep interior magnetic field strength becomes strong enough to stabilize interior regions of

the star against convection ($\nu \sim 10^{-4}$) that significant structural changes occur (as with the Gaussian radial profile). When this occurs, a large radiative shell appears in the interior, as shown by the inset in Figure 10. This radiative shell extends over 54% of the star by radius (between $0.18\,R_\star$ and $0.72\,R_\star$) and 78% by mass (between $0.03\,M_\star$ and $0.81\,M_\star$). We verified this was the dominant reason for structural changes by looking at the profile of a dipole radial profile model with a similar surface magnetic field strength. The $(\nabla_s - \nabla_{ad})$ profile exhibited in the surface layers by the dipole model is nearly identical to the Gaussian model. However, a radiative shell develops deep in the Gaussian model. This supports the idea that fully convective stars require radiative zones to be consistent with observations (Cox et al. 1981; Mullan & MacDonald 2001).

A model with the constant Λ profile has a slightly different $(\nabla_s - \nabla_{ad})$ profile in the super-adiabatic layer. It also produces a marginally larger surface radiative zone than the standard non-magnetic model. Convection in the deep interior is relatively unaffected, so a radiative core does not develop. We opted to not display these features in a figure because the overall profile is almost identical to the non-magnetic profile in Figure 10. Given the insensitivity of the overall stellar structure of fully convective stars to the size of the super-adiabatic layer, the constant Λ models have a negligible influence on the stellar radius.

4.2. Surface Magnetic Field Strengths

Surface magnetic field strengths are estimated from X-ray luminosity, L_x, measurements using the relation between total unsigned magnetic flux, Φ, and L_x derived by Feiden & Chaboyer (2013). We are unable, however, to estimate a reliable magnetic field strength for Kepler-16 B as it does not appear in the ROSAT catalogs. In a moment, we will provide at least a reasonable upper bound, but it is easiest to first address CM Dra.

The ROSAT Bright Source Catalogue (Voges et al. 1999) indicates that CM Dra has an X-ray count rate of $X_{cr} = 0.18 \pm 0.02$ counts s^{-1} with a hardness ratio of HR $= -0.30 \pm 0.07$. This translates into an X-ray luminosity per star of $L_x = (1.57 \pm 0.40) \times 10^{28}$ erg s^{-1}, where we have used a parallax of $\pi = 68 \pm 4$ mas (Harrington & Dahn 1980). Note that the X-ray luminosities are upper limits due to possible X-ray contamination in the ROSAT data. There are several stars nearby to CM Dra in the plane of the sky, but it is difficult to judge whether they contribute to the ROSAT count rate.

From the X-ray luminosity derived above, we find $\log_{10}(\Phi/\text{Mx}) = 24.81 \pm 0.45$. Errors associated with the surface magnetic field strength estimates are substantial due to the large error on the surface magnetic flux. Converting magnetic fluxes to surface magnetic field strengths, we estimate that $\langle Bf \rangle_A = 1.65^{+3.00}_{-1.07}$ kG and $\langle Bf \rangle_B = 1.85^{+3.36}_{-1.19}$ kG for CM Dra A and B, respectively. Note that quoted uncertainties are mean uncertainties. These estimates imply that the 6.0 kG surface magnetic field strengths predicted by our Gaussian radial profile models are likely too strong. However, this does not invalidate the magnetic field models, only our choice of radial profile. The magnetic field strength in the deep interior is of greater consequence, so it may be possible to construct a radial profile to greater reflect this fact.

Models that use a constant Λ formalism predict surface magnetic fields strengths up to ~ 3.0 kG. This upper limit is set by the magnetic field coming into equipartition with kinetic energy of convective flows (Chabrier & Küker 2006; Browning 2008). Values of 3.0 kG are consistent with our X-ray

estimated field strengths. Additionally, equipartition magnetic field strengths are consistent with typical average magnetic field strengths measured at the surface of M-dwarfs (Saar 1996; Reiners & Basri 2009; Shulyak et al. 2011; Reiners 2012). Although magnetic field strengths are consistent with observations, our models are unable to produce radii consistent with these realistic field strengths.

Although there are no X-ray measurements from ROSAT for Kepler-16, we can attempt to derive a reasonable estimate. From photometry, we may estimate a distance to Kepler-16 by assuming that the primary contributes to most of the observed flux in the visible. We estimate a distance of about 60 pc using the temperature and luminosity provided by (Doyle et al. 2011) and Winn et al. (2011) in combination with a bolometric correction from the PHOENIX model atmospheres. If we make the assumption that all of flux at X-ray wavelengths is from the secondary (recall the primary shows only weak magnetic activity; Winn et al. 2011), then taking the ROSAT sensitivity limit of $X_{cr} = 0.005$ counts per second (Voges et al. 1999), we find $L_x \sim 2 \times 10^{28}$ erg s^{-1}. This also assumes HR $= -0.1$, typical for dwarf stars. Converting to an unsigned magnetic flux yields $\log_{10}(\Phi/\text{Mx}) \sim 25$, or a magnetic field strength of the order of 2 kG for Kepler-16 B. Therefore, Kepler-16 likely does not have a magnetic field strength any larger than that found on the surface of CM Dra. Furthermore, if Kepler-16 B is rotating pseudo-synchronously, like it's companion, then it would have a rotation velocity $v \sin i < 0.5$ km s^{-1}, as mentioned in Section 1. CM Dra, on the other hand, has $v \sin i \sim 9.0$ km s^{-1}. Kepler-16 may very well have a weaker magnetic field, owing to its longer orbital (and presumably rotational) period. Therefore, we believe that the 6.0 kG surface magnetic field required to bring our models into agreement with observations is too strong.

4.3. Comparison to Previous Studies

Previous attempts to reconcile model radii with the observed radii of fully convective stars have focused solely on CM Dra, as it was the only well-studied system known (Chabrier et al. 2007; Morales et al. 2010; MacDonald & Mullan 2012). In each case, magnetic fields and magnetic activity were found to provide an adequate solution, which is quite the opposite conclusion from results presented in Section 3. This seeming contradiction of previous results can be understood by our neglect of star spots, in particular, the potential for observed radii to be over-estimated on a spotted star. Before submitting that spots are the solution and calling this case closed, we will review existing results, placing ours into context, and then provide an assessment of the magnetic hypothesis.

4.3.1. Summary of Methods and Key Results

Methods used in previous studies were, in some respects, similar. Each used a method for treating magneto-convection. Four techniques have been employed thus far: a reduced-α_{MLT} approach (Chabrier et al. 2007; Morales et al. 2010), stabilization of convection by a vertical magnetic field (MacDonald & Mullan 2012), stabilization by a more general magnetic field (not specifically vertical; this work), and then a turbulent dynamo approach that is similar to a reduced-α_{MLT} (this work). Including effects of star spots is inherently difficult in a 1D stellar evolution code. Spots are blemishes scattered across the stellar surface that extend a non-fixed distance into the surface convection zone. Spots have largely been treated in the same fashion in previous investigations and rely on reducing the total

stellar surface flux by a fractional amount,

$$\beta = \frac{S_{\text{spot}}}{S}\left[1 - \left(\frac{T_{\text{spot}}}{T_{\text{phot}}}\right)^4\right], \qquad (5)$$

where S_{spot}/S is the surface areal coverage of spots and $T_{\text{spot}}/T_{\text{phot}}$ is the spot temperature contrast. This approach is based on the "thermal plug" spot model advanced by Spruit (1982a, 1982b) and Spruit & Weiss (1986). The modified surface flux is then $\mathcal{F} = (1 - \beta)\mathcal{F}_{\star}$, where $\mathcal{F}_{\star}$ is the flux of the star if the photosphere is spot free.

Morales et al. (2010) performed a detailed analysis to establish how specific star spot properties effect results from both theoretical modeling and light curve analyses. For a given star spot β and assumed distribution of spots over the stellar surface (uniform, clustered at mid-latitudes, and clustered at the poles), they evaluated the reliability of light curve analyses in determining stellar radii. If spots are preferentially located at the poles, they showed that stellar radii may be over-estimated by as much as 6%. On the other hand, if spots are more evenly distributed across the surface, or clustered at mid-latitudes, radius determinations proved reliable for $\beta < 0.3$.

Combining the aforementioned results with the influence of spots on stellar evolution models, via Equation (5), Morales et al. (2010) found that $\beta = 0.17$ was required to fit the stars of CM Dra. Magneto-convection using a reduced-α_{MLT} was found to be ineffective and was not required. Thus, they predict that the stars in CM Dra are 35% covered by spots that are 15% cooler than the surface (this latter value was fixed in their analysis). This was deemed sufficient to correct model radii with observations.

MacDonald & Mullan (2012), on the other hand, were able to produce agreement between their model and observations using a combination of magneto-convection and star spots. They identified regions of $\delta_{\text{MM}} - \beta$ ($\beta \equiv f_s$ in their paper) parameter space that reconciles their models with CM Dra (see their Figures 13–15). Their magnetic inhibition parameter is defined as

$$\delta_{\text{MM}} = \frac{B^2}{B^2 + 4\pi\gamma P_{\text{gas}}}, \qquad (6)$$

where B is the magnetic field strength, γ is the ratio of specific heats, and P_{gas} is the total gas pressure. This quantity is added directly to the adiabatic gradient in the Schwarzschild stability criterion. What strongly distinguishes the MacDonald & Mullan (2012) study from the Morales et al. (2010) investigation is that MacDonald & Mullan (2012) do not include model inflation due to spots as described by Equation (5). Instead, they only adopt the adjustment made to the observed stellar radii due to the influence of polar spots on the light curve analysis. Model radius inflation is then caused by stabilization of convection using their inhibition parameter described above.

The full range of values for which they find agreement is $0.15 \lesssim \beta \lesssim 0.28$ with $0.0 < \delta_{\text{MM}} < 0.025$. To further constrain the parameter space, they assume the best-fit star spot $\beta = 0.17$ from Morales et al. (2010). This narrows the acceptable range for the magnetic inhibition parameter to $0.020 < \delta_{\text{MM}} < 0.025$. These values of δ_{MM} correspond to vertical magnetic field strengths of approximately 500 G at the stellar photosphere and a (capped) interior vertical magnetic field strength of 1 MG.

Our modeling results are largely consistent with those of Morales et al. (2010) and MacDonald & Mullan (2012). Comparing first with MacDonald & Mullan (2012), we focus on the dipole and Gaussian radial profile models with a rotational dynamo (Figures 8(a) and (b)). The magnetic perturbation applied

in these models is qualitatively similar to magneto-convection method favored by MacDonald & Mullan (2012). We have estimated that our magnetic field strengths should be up to an order of magnitude larger than those of Mullan & MacDonald (2001) as a consequence of our formulation (Feiden & Chaboyer 2013). Our "inhibition parameter" is primarily controlled by the quantity,

$$\nu\nabla_{\chi} = \frac{P_{\text{mag}}}{P_{\text{gas}} + P_{\text{mag}}}\left(\frac{d\ln\chi}{d\ln P}\right), \qquad (7)$$

where ν is a magnetic compression coefficient and ∇_{χ} is the gradient of the magnetic energy per unit mass with respect to the total pressure. We showed that $\nu \sim \delta_{\text{MM}}$ (Feiden & Chaboyer 2013), but our formulation has the additional term $\nabla_{\chi} \sim 0.1$. Therefore, to achieve the same results as MacDonald & Mullan (2012), we should need ν to be about 10 times larger than δ_{MM}. Thus, our requirement of a 6.0 kG surface magnetic field strength with a roughly 40 MG peak magnetic field strength for the Gaussian radial profile is consistent with the values we would expect given the values from MacDonald & Mullan (2012). Although the dipole radial profile model has a 5.0 kG surface magnetic field strength, the peak magnetic field strength is only 1.5 MG, a factor of 10 or so too small to impart the necessary structural changes.

To compare with Morales et al. (2010), we refer to our constant Λ models, which closely match the reduced-α_{MLT} formulation. We found that even if the magnetic field were a considerable fraction of the equipartition magnetic field strength ($\Lambda = 0.9999$), there is little impact on the stellar radii. This is consistent with Morales et al. (2010), who found that reducing α_{MLT} has a negligible impact on the stellar model predictions for fully convective stars, especially after star spots were invoked. In that sense, we confirm that reducing convective efficiency does not appear to be a viable method to fully account for inflation among fully convective stars.

Note that we have not adopted the reduced stellar radius presented by Morales et al. (2010) nor have we explicitly addressed reductions in surface flux due to star spots. Models presented in Feiden & Chaboyer (2013) did not require star spots to provide an adequate fit to the data. This reinforces a known degeneracy between magneto-convection implementations and introducing star spots (MacDonald & Mullan 2010). One may not be too surprised that these two issues are so closely connected, as spots are the physical manifestation of suppressed convection near the stellar surface. Therefore, it is reasonable to assume that reduction in convective flux from either magneto-convection or star spots should produce similar results. The degeneracy, in a sense, can be broken by the idea that star spots could bias light curve analyses toward larger radii. Magneto-convection, strictly speaking, has no influence on the light curve analysis, if we assume global changes to stellar properties. In that sense, particular configurations of spots (clustered near the pole) could have a significantly larger impact on the mass–radius problem than magneto-convection.

Despite the aforementioned results that support the magnetic field hypothesis, we are skeptical of the interpretation that magnetic fields are driving the observed radius inflation. We will now assess the results primarily by considering available observational data.

4.3.2. Assessment of Magneto-convection

Reductions in convective efficiency appear to be inadequate for producing the observed stellar radii (Section 3 of this work;

Chabrier et al. 2007; Morales et al. 2010). We showed that for Kepler-16 and CM Dra, radius inflation induced by the inhibition of convective efficiency was effectively negligible (∼0.1%). This is in agreement with Chabrier et al. (2007) and Morales et al. (2010), who find reducing the convective mixing length from $\alpha_{\mathrm{MLT}} = 2.0$ to $\alpha_{\mathrm{MLT}} = 0.1$ has little effect on the radii of fully convective stars. Reducing α_{MLT} further could begin to provide reasonable effects on fully convective stellar radii. The question then becomes, "is it possible for $\alpha_{\mathrm{MLT}} \to 0$, and if so, by what mechanism?"

Results from the stabilization of convection are encouraging. A proper amount of radius inflation can be achieved with somewhat reasonable surface magnetic field strengths (Section 3 of this work; MacDonald & Mullan 2012). Instead of surface field strengths posing a problem as they did with partially convective stars (Feiden & Chaboyer 2013), it is the interior magnetic field strengths, which range from 1 MG to 50 MG, that require attention.

There is presently no observational evidence to suggest a 1 MG (or greater) magnetic field could exist within a fully convective star. To be fair, there is also no direct evidence to rule out the possibility. We must be honest about the lack of observational data concerning interior magnetic field strengths. However, there is some indirect evidence that casts doubt on the existence of super-MG interior magnetic fields. We will now carefully examine the possibility that such fields do exist deep in fully convective stars.

From a theoretical perspective, there is concern about how a super-MG magnetic field is generated. Simulations suggest that turbulent dynamos reach saturation at field strengths of ∼50 kG (Chabrier & Küker 2006; Dobler et al. 2006; Chabrier et al. 2007; Browning 2008), two orders of magnitude below the 1 MG magnetic field required by stellar models. We will return to this a bit later. For now, let us assume that super-MG magnetic fields cannot be generated by dynamo action. Instead, it could be assumed that super-MG magnetic fields are the result of the amplification of a primordial μG seed magnetic field during the proto-stellar collapse.

Assuming magnetic flux is conserved during collapse of the proto-star, one finds that super-MG magnetic fields could plausibly exist. However, the super-MG magnetic fields must then survive several Gyr within the stellar interior without decaying. There are three primary timescales of interest: that given by macroscopic diffusion in a non-convecting medium, the rise time for a buoyantly unstable flux tube, and the advection timescale in a convecting medium with relatively high conductivity. We'll consider the latter, first.

If the stellar plasma is highly conducting, which is a valid assumption throughout the interior of stars, then the field lines will be frozen into the plasma. We might then expect that the flux tubes will be carried by convection from deep within the star to the stellar surface, where the they will then dissipate their energy. The timescale for this to occur is roughly $\tau_{\mathrm{conv}} = R_\star/u_{\mathrm{conv}}$, where $R_\star \sim 10^{10}$ cm and $u_{\mathrm{conv}} \sim 10^3$ cm s^{-1}. We find that $\tau_{\mathrm{conv}} \sim 10^7$ s, or about 1 yr. Even if we assume $u_{\mathrm{conv}} \sim 10^1$–$10^2$ cm s^{-1}, $\tau_{\mathrm{conv}} \sim 10^8$–$10^9$ s. Thus, the timescale for this type of advection is about 10 yr. Although convection can quickly carry a flux tube from the deep interior to the stellar surface, the process can also carry flux tubes from the surface to deep in the interior.

A more unidirectional process that can transport magnetic flux to the stellar surface is the magnetic buoyancy instability (e.g., Parker 1955, 1979). Magnetic flux tubes are assumed to

be in pressure equilibrium with their surroundings deep in the interiors of stars,

$$p_{\mathrm{gas},\,i} + \frac{B^2}{8\pi} = p_{\mathrm{gas},\,e}, \tag{8}$$

where $p_{\mathrm{gas},\,i}$ and $p_{\mathrm{gas},\,e}$ are the interior and exterior gas pressures acting on the flux tube, respectively, and $B^2/8\pi$ is the magnetic pressure within the flux tube. Since flux tubes are supported by both the internal gas pressure and the magnetic pressure, the gas density within a flux tube is lower than the surrounding gas density, provided that the temperature inside the flux tube is the same as the temperature of the surroundings. This density perturbation creates a buoyancy force toward the surface of the star, but will be counteracted by radially inward hydrodynamic forces resulting from convective down-flows.

If we assume a polytropic EOS, a reasonable approximation for deep stellar interiors, and that p_{gas} can be expressed as a power-series expansion about $\rho_{\mathrm{gas},\,e}$, the gas density exterior to the flux tube, then truncating the series to first order gives

$$p_{\mathrm{gas},\,e}\left[1 + \gamma \rho_{\mathrm{gas},\,e}^{-1}\Delta\right] + \frac{B^2}{8\pi} = p_{\mathrm{gas},\,e}, \tag{9}$$

where γ is the ratio of specific heats and $\Delta = \rho_{\mathrm{gas},\,i} - \rho_{\mathrm{gas},\,e}$ is the density perturbation. The specific buoyancy force resulting from this density perturbation is

$$f_b = \frac{g}{\gamma}\left(\frac{B^2}{8\pi p_{\mathrm{gas},\,e}}\right). \tag{10}$$

Balancing the buoyancy force with the hydrodynamic force (Fan 2009) yields the condition whereby a magnetic flux tube will be unstable to buoyant rise,

$$B \gtrsim \left(\frac{H_P}{a}\right)^{1/2} B_{\mathrm{eq}}, \tag{11}$$

where B is the magnetic field, H_P is the local pressure scale height, a is the flux tube radius, and B_{eq} is equipartition magnetic field given in Section 2.2.4. This is a simplified picture that ignores effects due to curvature and the response of the magnetic tension that may act to prevent the onset of buoyant instability. However, it provides a reasonable order of magnitude approximation. Given the propensity for magnetic stellar models to invoke magnetic fields with $B \geqslant 10^6$ G, we can estimate a typical flux tube radius needed to maintain this magnetic field strength stable against buoyancy.

For M-dwarfs, $H_P \sim 10^9$ cm and $B_{\mathrm{eq}} \sim 10^4$ G. Thus, to maintain strong 10^6 G magnetic fields deep in the interior (as in MacDonald & Mullan 2012), flux tubes must be no larger than 10^5 cm, or 1 km. This means the ratio of the pressure scale height to the flux tube radius must be ∼10^4. By comparison, the values estimated for this ratio near the solar tachocline are of the order of unity (Fan 2009). This ratio rises to 10^6 ($a \sim 10$ m) if the deep interior magnetic field is to be of the order of 10^7 G (this work). Once the flux tube becomes unstable to buoyant rise, an estimate of the rise time can be approximated assuming that the tube travels at the Alfvén velocity (Parker 1975). A 10^6 G magnetic field will traverse a stellar radius $R \sim 10^{10}$ cm in approximately $10^{5.5}$ s, or about 10 days, assuming a constant density of 10^2 g cm^{-3}. This rise time will be increased by non-adiabatic heating effects, but remains small compared to evolutionary timescales (Parker 1974).

Figure 10 indicates that a radiative shell develops deep within the star in the presence of a super-MG magnetic field. This means that the dissipation time of the magnetic field does not necessarily obey the advection timescale discussed above. Instead, we may look at the timescale for diffusion given by the induction equation. In the absence of any favorable current networks, we have that

$$\frac{\partial \mathbf{B}}{\partial t} = \eta \nabla^2 \mathbf{B}, \qquad (12)$$

where η is the magnetic diffusivity. The approximate timescale for diffusion, assuming $\eta \sim 10^2$–10^3 cm^2 s^{-1} (Chabrier et al. 2007), is then $\tau_{\rm diff} \sim L^2/\eta$, where L is the size of the radiative shell. The field diffuses through the radiative shell until it reaches the convective boundary, which then efficiently transports magnetic flux to the stellar surface. Based on our models of CM Dra, we find the size of radiative shell is $L \sim 10^{10}$ cm. Therefore, $\tau_{\rm diff} \sim 10^{10}$–$10^{11}$ yr, assuming the magnetic field fully diffuses out of the radiative zone. However, even within a radiation zone, magnetic buoyancy must be considered and can lead to a rapid rise time for magnetic flux tubes (e.g., MacGregor & Cassinelli 2003).

These are only order of magnitude approximations, so it is possible that the field could survive for a shorter or longer time in any scenario. Instead, this exercise suggests that an amplified seed field, or any super-MG magnetic field, present in a fully convective star will likely decay away rapidly owing to the magnetic buoyancy instability. We note that this is still possible, even if a sizeable radiative zone develops as a result of the strong magnetic field. Furthermore, the radiative zone is a product of the magnetic field and therefore exists in an unstable equilibrium. As the magnetic field decays away, so will the radiative zone.

MacDonald & Mullan (2012) recognized that primordial magnetic fields would likely decay and thus were not a suitable solution for the existence of super-MG magnetic fields within CM Dra. Instead, they proposed that the dynamo mechanism may be able to generate the necessary magnetic fields. Their proposal contradicts what we mentioned earlier, that simulations are unable to generate magnetic fields greater than $\sim$50 kG in fully convective models. MacDonald & Mullan (2012) reason that this is a result of those simulations using rotational velocities similar to those in the Sun. If one nominally assumes that magnetic field strengths increase with rotation rate, then a star like CM Dra will have considerably stronger magnetic fields than does the Sun.

Using a scaling relation between magnetic field strength and rotational angular velocity, MacDonald & Mullan (2012) find that CM Dra should have a surface magnetic field strength of about 500 G with an internal magnetic field strength anywhere between 0.3 MG and 1.3 MG. This could then explain the existence of super-MG magnetic field strengths. Note that the magnetic field strength is predicted to be the large-scale magnetic field strength, not necessarily the total magnetic field strength.

However, the peak interior magnetic field strength seen in simulations is moderated by the kinetic energy available in convective flows. This was discussed in Section 2.2.4. Simulations find that a dynamo driven by turbulent convection can create both small-scale magnetic fields and large-scale magnetic fields (Chabrier & Küker 2006; Browning 2008). It is not immediately clear that rotation would not drive stronger magnetic field strengths, so we will proceed in our discussion

assuming that it might to see if we encounter any inherent contradictions.

The scaling relation adopted by MacDonald & Mullan (2012) would then also explain why KOI-126 can be fit by stellar evolution models. KOI-126 is a triply eclipsing system found earlier in the *Kepler* data (Carter et al. 2011) that contains two fully convective stars that are nearly identical to CM Dra. Yet, the properties of KOI-126 (B, C) are well reproduced by standard stellar evolution models (Feiden et al. 2011; Spada & Demarque 2012). Assuming a scaling relation between magnetic field strength and rotational angular velocity may support this finding. KOI-126 (B, C) have an orbital period of 1.77 days, to be compared to the 1.27 day orbit of CM Dra. This 0.5 day difference in orbital period means KOI-126 (B, C) would have weaker magnetic fields than CM Dra and would experience considerably less radius inflation (MacDonald & Mullan 2012).

MacDonald & Mullan (2012) predict that KOI-126 should be inflated by approximately 2%–3%. We find this difficult to understand in context of the agreement between standard stellar evolution models and the observed radii. Inflating model radii by 2%–3% would mean that models would over-predict the radii of KOI-126 (B, C). If one assumes that spots are biasing the observed radius measurements, it would decrease the measured radii, again breaking the agreement between the observations and the models. There seems to be problems with simultaneously increasing model radii and decreasing the measured radii of KOI-126 (B, C) while still maintaining model-observation agreement.

Furthermore, the scaling relation suggested to validate super-MG magnetic fields may not be compatible with observations. Results seem to show that at a given mass, the large-scale magnetic field strength of fully convective stars do not appear to depend on rotation below a critical threshold (see, e.g., Figure 3 in Donati & Landstreet 2009). For low-mass stars, this threshold corresponds to a rotation period of about 3 or 4 days. Magnetic field saturation is also observed in data regarding the total magnetic field strength of fully convective stars. Magnetic fields saturate around 3 kG for $v \sin i > 3$ km s^{-1} (Reiners et al. 2009; Shulyak et al. 2011). Saturation inherently implies that scaling relations are invalid. Since both CM Dra and KOI-126 (B, C) have components rotating faster than the threshold for saturation, there is no reason to assume that their magnetic fields are that different. There is the possibility that their large-scale components (and thus vertical) magnetic fields are sufficiently different, but this is not immediately obvious.

Finally, we note that magneto-convection techniques alone have not been sufficient to rectify the model-observations disagreements. Effects of star spots must be included and must therefore be assessed on their own basis.

4.3.3. Assessment of Star Spots

The most efficient means of inflating low-mass stellar models of CM Dra is by including star spots (Morales et al. 2010; MacDonald & Mullan 2012). Although we did not explicitly include spots, we will take a careful look at the results of these two previous studies. We feel this analysis is required in light of recent observational data, including confirmation that CM Dra has a sub-solar metallicity of [Fe/H] $\approx -0.3 \pm 0.1$ (Rojas-Ayala et al. 2012; Terrien et al. 2012).

We use approximate fits to the Morales et al. (2010) spot-modeling results to estimate how a metallicity reduction alters their conclusions. Assuming polar spots, they find that spots tend to bias observations toward larger radii. From the few data
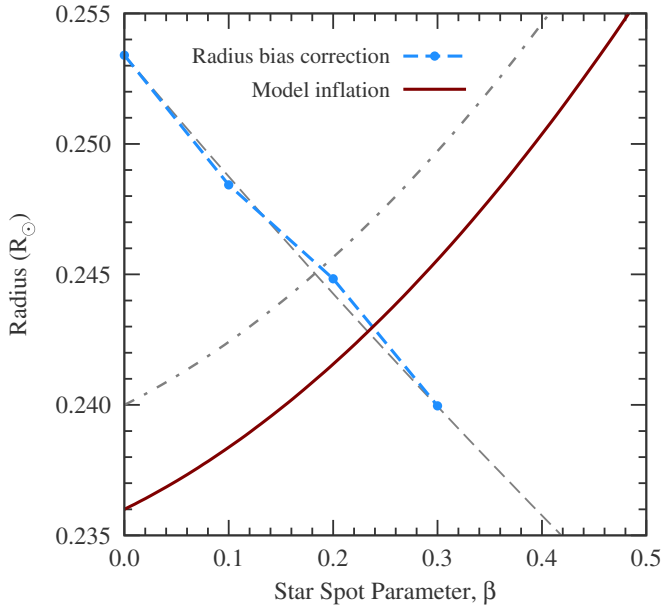
Figure 11. Effects of star spots on DEB radius measurements and on stellar evolution model radii. Data points in light-blue, connected by a dashed line, show the downward corrected radius for CM Dra A in the presence of polar spots. Data are taken directly from Figure 7 in Morales et al. (2010) for a polar spot distribution. The light-gray dashed line is a linear fit to the data given in Equation (13). The solid maroon curve illustrates how model radii increase with spot coverage.

(A color version of this figure is available in the online journal.)

points in their Figure 7, we calculate that spots produce larger radii according to the function

$$R_{\rm spot}/R_{\rm real} = 0.187\beta + 1.0, \tag{13}$$

where $R_{\rm spot}/R_{\rm real}$ is the ratio of the radius derived when polar spots are present to the actual radius. This function can be used to correct for the radius bias produced by spots. In stellar models, spots can also increase radius predictions. Given the data in Figure 8 of Morales et al. (2010), model radii can be approximated as,

$$R/R_\odot = R_0(0.172\beta^2 + 0.0834\beta + 1.0) \tag{14}$$

where R_0 is the radius of a non-magnetic model in units of solar radii. We note that this formula approximates the effects of spots only for model masses of $\sim 0.23\,M_\odot$. The intersection of these two relations in the β–R plane provides an estimate of the star spot parameter required to correct models.

Figure 11 illustrates that a model of CM Dra A with [Fe/H] = −0.3 (see also Figure 7) needs a star spot $\beta \sim 0.19$ to match observations. Small differences in our results from those of Morales et al. (2010) are due to the adopted base model (Dartmouth versus Lyon) and our method of fitting polynomials to the spot radius bias and inflation data in Morales et al. (2010). Changing β has a proportionally larger effect on correction for radius measurement biases than it does on inflation caused in stellar models. If this correction is not applied, $\beta = 0.38$ is needed to produce agreement using model radius inflation at sub-solar metallicity.

Whether the required star spot parameter is realistic is a more difficult question. Spot properties for M-dwarfs are relatively unconstrained, as identifying spot sensitive features in spectra is complicated by uncertainties in modeling molecular features.

Nonetheless, there are three components to the spot parameter that are of interest: spot coverage, spot temperature contrast, and spatial distribution. We will address each separately and then present a unified picture afterward.

Temperature contrast. Spot temperature contrast is defined, here, to be the ratio of the spot temperature to the temperature of the unblemished stellar photosphere. As seen from Equation (5), constraining the spot temperature contrast provides insight into the required filling factor predicted by the spot model. Although no direct empirical constraints exist for M-dwarfs, there have been studies performed to measure spot temperature contrasts of K stars using TiO bandhead features (O'Neal et al. 1998, 2004). We will take a closer look at those results, here.

Properties of spots were determined by fitting the shape of TiO bandheads with a spectrum created using a two temperature spot model. This technique involves convolving two template spectra for which the effective temperature is assumed to be known and finding the best combination of template spectra to produce the molecular bandhead features in spectra of a given star (see, e.g., O'Neal et al. 1998). The result is an estimate of the temperatures for the unblemished photosphere and the spotted regions, as well as the fractional surface coverage of each feature (see below). Using this technique, it was found that active K stars—specifically II Peg and EQ Vir—have spots with a characteristic temperature contrast of 75% (25% cooler than the unblemished photosphere).

This estimate, however, relies on the temperature for the two template spectra being correct. Results from interferometric studies (e.g., Boyajian et al. 2012) have revised the temperature estimates for the stars whose spectra were used as templates in the O'Neal et al. investigations. These revisions only affect the temperatures for template spectra used as the spot (cool) component in the fit, namely, the temperatures associated with cooler M-dwarf spectra, and increase the associated effective temperature by 300 K–400 K. Taking into account the revised temperature scale for the cooler template spectra, one finds the temperature contrast for K stars inferred from molecular bandhead features is between 82% (II Peg) and 90% (EK Vir). The warmer spot temperatures are supported by Doppler Imaging (DI) studies of II Peg, which indicate temperature contrasts between 80% and 85% (Hackman et al. 2012).

Assuming that spot temperature contrasts become weaker toward later spectra types (Berdyugina 2005), then one might expect M-dwarfs to have spot temperature contrasts around 90% (10% cooler than the unspotted surface). Using this value, one finds that a spot surface coverage of 55% is required to satisfy the condition that $\beta = 0.19$ for CM Dra. Of course, slightly warmer or cooler spots may be permitted, depending on the efficiency at which spots temporarily suppress surface convection. For the sake of argument, we take 90% to be a typical spot contrast. We now look whether a spot areal coverage of 55% is consistent with empirical evidence.

Surface coverage. To assess what constitutes typical spot surface coverages, we look to results from DI and molecular bandhead fitting. Using DI, spot coverages for three M-dwarfs have been estimated. DI maps of HK Aqr, RE 1816+541, and V374 Peg (Barnes & Collier Cameron 2001; Barnes et al. 2004; Morin et al. 2008) reveal varying levels of surface coverage from 2% (V374 Peg) up to 40% (HK Aqr). Similarly, surface coverages derived by modeling the shape of TiO bandheads of active K stars—again II Peg and EK Vir—are typically around 30%–40%, consistent with values found in DI investigations (O'Neal et al. 1998, 2004). There are no measurements of spot

coverages on M-dwarfs using this technique, which limits the applicability of these results, but we may cautiously extrapolate and assume that M-dwarfs are able to possess at least similar surface coverages.

For one of the K stars studied using the molecular bandhead technique, II Peg, information on spot coverage from DI is also available. Hackman et al. (2012) mapped the spot coverage of II Peg and find seasonal variation in spot coverage between 5% and 20%, a factor of eight and two lower than the coverage inferred from TiO bandheads, respectively. Seasonal variation is expected if magnetic activity cycles are present in other stars, so it's not surprising that one observes this phenomenon. However, the difference between the maximum surface coverage revealed by DI (20%) and that obtained using molecular bandhead features (40%) highlights a known limitation with DI studies: they are only sensitive to spot features larger than the grid resolution in the DI analysis. In other words, small-scale spot features will be missed by the DI reconstruction. This is especially relevant since comparison of spectro-polarization measurements of M-dwarf magnetic fields using Stokes I and V polarization indicate a majority of the magnetic energy is contained in small-scale features (Reiners & Basri 2009). Therefore, spot coverages inferred from DI maps must be taken as lower limits to the true spot coverage. One may then plausibly expect spot surface coverages at least as high as 40% for M-dwarfs.

Evidence from both DI and molecular bandhead fitting support the existence of spot coverages around 40% for active late K-dwarfs and M-dwarfs. This is below the 55% needed to satisfy the use of a $\beta = 0.19$ spot parameter. Whether 55% is *unrealistically* high is unclear. If, for instance, the spot temperature contrast were around 85%, as opposed to 90%, then the required spot surface coverage would be 40%, and thus consistent with observations. One could just as well argue the opposite, that a larger temperature contrast of 94% would require a surface coverage of 87% and push the requirement further from the current empirical evidence.

One further scenario is that stars are able to achieve spot coverages near 100%. Observations suggest that the filling factor of magnetic fields at the surface of fully convective stars (both main-sequence and pre-main-sequence) approaches unity (Johns-Krull et al. 2004; Shulyak et al. 2011; Johnstone et al. 2014). We must then try to understand the connection between the presence of magnetic fields and star spots. This includes determining how strong of a magnetic field is necessary at the surface of an M-dwarf to generate spots of appreciable temperature contrast. It may be that pervasive 1 kG magnetic fields covering the whole surface of fully convective stars may be too weak to cause any noticeable effects on convection. Such an even distribution of small spots would also likely not cause any noticeable light curve modulation, if filling factors approach unity. However, pockets of strong 5–8 kG magnetic fields (Shulyak et al. 2011) may produce the noticeable light curve modulation, bias stellar radii measurements, and suppress surface convection.

Spatial distribution. Arguably, whether spots cluster near the poles of active M-dwarfs is of greatest consequence for the present assessment. Evidence for spots clustered at the poles is less definitive than temperature contrasts and surface coverages. About half of all stars studied using DI show signs of polar caps (Berdyugina 2005). Exceptions are very active stars and M-dwarfs, which tend to have spots distributed across all latitudes. Of the three DI spot maps generated for M-dwarfs,

none display evidence for polar caps (Barnes & Collier Cameron 2001; Barnes et al. 2004; Morin et al. 2008). A DI study of CM Dra to search for possible signs of significant polar coverage of spots is needed. Ideally, this would be performed with existing data that was used to derive the stellar properties, but a look at the signal to noise of the observations reveals that the data is likely unsuitable for such an investigation (see Metcalfe et al. 1996). In the meantime, we must be cautious as even polar spots would require large areal coverages (half or more of the stellar surface) to provide agreement between models and observations.

Additional evidence for non-polar-cap distributions comes from studies of the $\sim$150 Myr open cluster NGC 2516. The statistical distribution of light curve modulations assumed to be caused by star spots in the low-mass star population can only be reproduced if the stars have randomized spot latitudinal distributions and rotational inclination angles (Jackson et al. 2009; Jackson & Jeffries 2013). We do note that these latter studies also require spot temperature contrasts of 75%, which we have just discussed may be too dramatic for K- and M-dwarfs. How using a more realistic spot contrast would alter their results is unclear as there are strong degeneracies when modeling spot modulation in light curves. A first estimate would be that typical surface coverages would increase from the $40\% \pm 10\%$ that was required in their study.

There is as yet no definitive empirical evidence for polar cap spots among fully convective main-sequence stars. However, there is a theoretical expectation that spots should be located near the poles in rapidly rotating stars (e.g., Schüssler & Solanki 1992; DeLuca et al. 1997). Whether this expectation applies to fully convective stars is questionable, as spots distributed more evenly at lower latitudes may be more reasonable for more distributed dynamos (DeLuca et al. 1997). Based on only three data points, the apparent lack of polar spots among fully convective main-sequence stars is not robust and requires further confirmation.

Is it then possible to abandon the idea of a largely polar cap distribution and still rely on spots to address the radius discrepancies? In Figure 11, we see that abandoning the idea of polar spots requires $\beta = 0.38$ if model inflation is to alone correct for the observed radii. In this case, a spot temperature contrast of 89% with areal coverage of 100% would be required. Temperature contrasts greater than 89% lead to areal coverages greater than 100% and are thus unphysical. Even as one approaches 100% surface coverage (for temperature contrasts below 89%), it becomes increasingly difficult to produce spot modulation in light curves as there are fewer regions of unblemished photosphere left to produce the asymmetries needed, as discussed in the previous section. Considering patches of varying spot temperature contrast may provide the necessary asymmetries, but has not yet been investigated for consistency with the empirical data.

4.3.4. Putting it all Together

The case for magnetic fields inflating the radii of fully convective stars appears to be tenuous. Stabilization of convection in stellar models can produce the necessary radius inflation with reasonable surface magnetic field strengths. However, the models require super-MG magnetic fields in the interior. We are hesitant to suggest that real stars contain such strong interior magnetic fields for several reasons.

First, turbulent dynamos cannot generate magnetic fields with strengths greater than about 50 kG (Dobler et al. 2006; Chabrier & Küker 2006; Browning 2008). How magnetic fields with

strengths greater than 1 MG would accumulate in the interior of fully convective stars would be unknown. If super-MG magnetic fields are of primordial origin, they would probably not survive to the present day. Nor would magnetic field strengths of that magnitude be generated within the star and survive on evolutionary timescales. To avoid this, one can assume a scaling relation between magnetic field strengths and rotation, as suggested by MacDonald & Mullan (2012) to explain the super-MG magnetic fields. However, this breaks down for most stars in DEBs. Observations indicate a saturation of magnetic flux for fully convective stars that have rotation periods below ∼2.5 days (Donati & Landstreet 2009; Reiners et al. 2009; Shulyak et al. 2011). Also, KOI-126 (B, C) agree with stellar evolution models (Feiden et al. 2011). These stars exist in a regime where magnetic flux saturation should occur, but are seemingly uninfluenced by the presence of any magnetic phenomena. If super-MG magnetic fields are causing dramatic inflation in CM Dra, one would expect to observe it in KOI-126 (B, C) as well. Finally, suppression of convective efficiency is unable to provide a suitable solution on its own. Instead, star spots may be invoked for fully convective stars, which introduces additional concerns.

The presence of star spots on the stellar surfaces may provide an adequate solution, mostly through biasing the analysis of light curve data. From observations, star spots on fully convective stars can be characterized as: having temperatures about 10% cooler than the surrounding photosphere (O'Neal et al. 1998, 2004; Berdyugina 2005; Hackman et al. 2012), having surface coverages ranging from a couple percent (Morin et al. 2008; Hackman et al. 2012) up to around 40% (Barnes & Collier Cameron 2001; Barnes et al. 2004; O'Neal et al. 1998, 2004), and having spot distributions that appear to be more random and not clustered at the poles.

At this point, there is not sufficient empirical data regarding spot properties of M-dwarfs to draw firm conclusions. Still, the lack of noticeable spots at the poles is a concern. Results regarding how spots bias radius measurements rely on concentrated regions of spot coverage at the poles that are darker than their surroundings. At present, this feature is not observationally supported, but more work needs to be performed on this matter.

5. SUMMARY

This paper addressed the question of whether magnetic fields can realistically inflate the radii of fully convective stars. We approached the problem by modeling two individual DEBs that contain fully convective stars, Kepler-16 and CM Dra. Our models showed that the observed radii could be reproduced provided that a strong 50 MG magnetic field resides deep within these fully convective stars. We proceeded to show that multiple mechanisms—advection due to convective flows, macroscopic diffusion, and magnetic buoyancy instability—can lead to rapid destruction of such strong magnetic fields. These estimates would benefit from detailed numerical simulations to probe further whether such magnetic fields can stably reside deep within M-dwarfs. An assessment of the hypothesis that star spots are responsible for the observed inflation was also given. Here, the hypothesis largely rests on the assumption that large conglomerations of spots lie near the poles; a prediction that has not yet been observed among main-sequence, fully convective stars.

After weighing the evidence, we find it difficult to favor the hypothesis that magnetic fields are actively inflating the radii of fully convective, main-sequence stars. There are numerous uncertainties that must be addressed on both the theoretical and observational side of the hypothesis. More sophisticated magneto-convection models are required to further investigate this issue, using both simplified 1D approximations and more detailed 3D MHD models. Most critical, though, will be observational studies of star spots and magnetic fields of low-mass stars. These properties must be further constrained by observations if we are to rule out any of the physical pictures presented by the current generation of 1D stellar evolution models. In the meantime, it may not be too early to start seeking other solutions.

REFERENCES

Andersen, J. 1991, A&ARv, 3, 91
Baraffe, I., Chabrier, G., Allard, F., & Hauschildt, P. H. 1998, A&A, 412, 403
Barnes, J. R., & Collier Cameron, A. 2001, MNRAS, 326, 950
Barnes, J. R., James, D. J., & Collier Cameron, A. 2004, MNRAS, 352, 589
Barnes, S. A. 2010, ApJ, 722, 222
Bender, C. F., Mahadevan, S., Deshpande, R., et al. 2012, ApJ, 751, L31
Berdyugina, S. V. 2005, LRSP, 2, 8
Boyajian, T. S., von Braun, K., van Belle, G., et al. 2012, ApJ, 757, 112
Browning, M. K. 2008, ApJ, 676, 1262
Carter, J. A., Fabrycky, D. C., Ragozzine, D., et al. 2011, Sci, 331, 562
Chabrier, G., & Baraffe, I. 1995, ApJ, 451, L29
Chabrier, G., & Baraffe, I. 1997, A&A, 327, 1039
Chabrier, G., Gallardo, J., & Baraffe, I. 2007, A&A, 472, L17
Chabrier, G., & Küker, M. 2006, A&A, 446, 1027
Chandrasekhar, S. 1961, Hydrodynamic and Hydromagnetic Stability (International Series of Monographs on Physics; Oxford: Clarendon)
Cox, A. N., Hodson, S. W., & Shaviv, G. 1981, ApJL, 245, L37
DeLuca, E. E., Fan, Y., & Saar, S. H. 1997, ApJ, 481, 369
Dobler, W., Stix, M., & Brandenburg, A. 2006, ApJ, 638, 336
Donati, J.-F., & Landstreet, J. D. 2009, ARA&A, 47, 333
Dotter, A., Chaboyer, B., Jevremović, D., et al. 2007, AJ, 134, 376
Dotter, A., Chaboyer, B., Jevremović, D., et al. 2008, ApJS, 178, 89
Doyle, L. R., Carter, J. A., Fabrycky, D. C., et al. 2011, Sci, 333, 1602
Durney, B. R., De Young, D. S., & Roxburgh, I. W. 1993, SoPh, 145, 207
Eggen, O. J., & Sandage, A. 1967, ApJ, 148, 911
Fan, Y. 2009, LRSP, 6, 4
Feiden, G. A. 2013, PhD thesis, Dartmouth College
Feiden, G. A., & Chaboyer, B. 2012a, ApJ, 757, 42
Feiden, G. A., & Chaboyer, B. 2012b, ApJ, 761, 30
Feiden, G. A., & Chaboyer, B. 2013, ApJ, 779, 183
Feiden, G. A., Chaboyer, B., & Dotter, A. 2011, ApJL, 740, L25
Gizis, J. E. 1997, AJ, 113, 806
Gough, D. O., & Tayler, R. J. 1966, MNRAS, 133, 85
Guenther, D. B., Demarque, P., Kim, Y., & Pinsonneault, M. H. 1992, ApJ, 387, 372
Hackman, T., Mantere, M. J., Lindborg, M., et al. 2012, A&A, 538, A126
Harrington, R. S., & Dahn, C. C. 1980, AJ, 85, 454
Hauschildt, P. H., Allard, F., & Baron, E. 1999, ApJ, 512, 377
Hut, P. 1981, A&A, 99, 126
Irwin, A. W. 2007, The Free EOS Code for Calculating the Equation of State for Stellar Interiors V: Improvements in the Convergence Method, http://freeeos.sourceforge.net/convergence.pdf
Irwin, J. M., Quinn, S. N., Berta, Z. K., et al. 2011, ApJ, 742, 123
Jackson, R. J., & Jeffries, R. D. 2013, MNRAS, 431, 1883
Jackson, R. J., Jeffries, R. D., & Maxted, P. F. L. 2009, MNRAS, 339, L89

Johns-Krull, C. M., Valenti, J. A., & Saar, S. H. 2004, ApJ, 617, 1204
Johnson, J. A., & Apps, K. 2009, ApJ, 699, 933
Johnstone, C. P., Jardine, M., Gregory, S. G., Donati, J.-F., & Hussain, G. 2014, MNRAS, 437, 3202
Kalirai, J. S., Saul Davis, D., Richer, H. B., et al. 2009, ApJ, 705, 408
Kuznetsov, M. K., Pavlenko, Y. V., Jones, H., & Pinfield, D. J. 2012, AASP, 2, 15
Lacy, C. H. 1977, ApJ, 218, 444
Leggett, S. K., Allard, F., & Hauschildt, P. H. 1998, ApJ, 509, 836
Limber, D. N. 1958, ApJ, 127, 363
López-Morales, M. 2007, ApJ, 660, 732
Lydon, T. J., & Sofia, S. 1995, ApJ, 101, 357
MacDonald, J., & Mullan, D. J. 2010, ApJ, 723, 1599
MacDonald, J., & Mullan, D. J. 2012, MNRAS, 421, 3084
MacGregor, K. B., & Cassinelli, J. P. 2003, ApJ, 586, 480
Martins, D. H. 1975, PASP, 87, 163
Metcalfe, T. S., Mathieu, R. D., Latham, D. W., & Torres, G. 1996, ApJ, 456, 356
Morales, J. C., Gallardo, J. J., Ribas, I., et al. 2010, ApJ, 718, 502
Morales, J. C., Ribas, I., & Jordi, C. 2008, A&A, 478, 507
Morales, J. C., Ribas, I., Jordi, C., et al. 2009, ApJ, 691, 1400
Morin, J., Donati, J. F., Forveille, T., et al. 2008, MNRAS, 384, 77
Mullan, D. J., & MacDonald, J. 2001, ApJ, 559, 353
O'Neal, D., Neff, J. E., & Saar, S. H. 1998, ApJ, 507, 919
O'Neal, D., Neff, J. E., Saar, S. H., & Cuntz, M. 2004, AJ, 128, 1802
Orosz, J. A., Welsh, W. F., Carter, J. A., et al. 2012, ApJ, 758, 87
Parker, E. N. 1955, ApJ, 121, 491
Parker, E. N. 1974, Ap&SS, 31, 261
Parker, E. N. 1975, ApJ, 198, 205
Parker, E. N. 1979, Cosmical Magnetic Fields: Their Origin and Their Activity (New York, NY: Oxford Univ. Press)

Piskunov, N. E., Kupka, F., Ryabchikova, T. A., Weiss, W. W., & Jeffery, C. S. 1995, A&AS, 112, 525
Popper, D. M. 1984, AJ, 89, 132
Reiners, A. 2012, LRSP, 8, 1
Reiners, A., & Basri, G. 2007, ApJ, 656, 1121
Reiners, A., & Basri, G. 2009, A&A, 496, 787
Reiners, A., Basri, G., & Browning, M. 2009, ApJ, 692, 538
Ribas, I. 2006, Ap&SS, 304, 89
Rojas-Ayala, B., Covey, K. R., Muirhead, P. S., & Lloyd, J. P. 2012, ApJ, 748, 93
Saar, S. H. 1996, in IAU Symp. 176, Stellar Surface Structure ed. K. G. Strassmeier & J. L. Linsky (Dordrecht: Kluwer), 237
Salaris, M., Cassisi, S., Pietrinferni, A., Kowalski, P. M., & Isern, J. 2010, ApJ, 716, 1241
Schüssler, M., & Solanki, S. K. 1992, A&A, 264, L13
Shulyak, D., Seifahrt, A., Reiners, A., Kochukhov, O., & Piskunov, N. 2011, MNRAS, 418, 2548
Spada, F., & Demarque, P. 2012, MNRAS, 422, 2255
Spruit, H. C. 1982a, A&A, 108, 348
Spruit, H. C. 1982b, A&A, 108, 356
Spruit, H. C., & Weiss, A. 1986, A&A, 166, 167
Stassun, K. G., Kratter, K. M., Scholz, A., & Dupuy, T. J. 2012, ApJ, 756, 47
Terrien, R. C., Fleming, S. W., Mahadevan, S., et al. 2012, ApJL, 760, L9
Thompson, W. B. 1951, PMag, 42, 1417
Torres, G., Andersen, J., & Giménez, A. 2010, A&ARv, 18, 67
Valenti, J. A., & Piskunov, N. 1996, A&AS, 118, 595
Viti, S., Jones, H., Maxted, P., & Tennyson, J. 2002, MNRAS, 329, 290
Viti, S., Jones, H. R. A., Schweitzer, A., et al. 1997, MNRAS, 291, 780
Voges, W., Aschenbach, B., Boller, Th., et al. 1999, A&A, 349, 389
Winn, J. N., Albrecht, S., Johnson, J. A., et al. 2011, ApJL, 741, L1
Zwicky, F. 1966, Sci, 153, 53